Chapter 10
Emission and Laser Spectroscopy of Trapped Highly Charged Ions in Electron Beam Ion Traps

José R. Crespo López-Urrutia and Zoltán Harman

Abstract Research with highly charged ions addresses bound state quantum electrodynamics and relativistic atomic theory at their frontiers. Electron beam ion traps have provided practical means to study not only these fundamental fields, but also the physics of extremely hot plasmas in stars, active galactic nuclei, and fusion research plasma devices. Starting from the X-ray region, where the first experiments took place, this chapter will visit various regions of the electromagnetic spectrum and give a review of essential contributions of different groups to this field.

10.1 Introduction

Wherever high concentrations of energy are present, be it inside stars, in active galactic nuclei containing black holes, or fusion devices, highly charged ions (HCI) play a dominating role in radiation transport. They also tenuously fill vast regions of space as the warm–hot intergalactic medium (WHIM). Knowledge of the spectroscopy of HCI is essential for diagnosing astrophysical plasmas. In HCI, the tightly bound active electrons show enormously magnified quantum electrodynamics, relativistic and nuclear size effects compared to their outer-shell counterparts in neutrals. Today, their accurate description still challenges theory, and their study offers new avenues for an improved understanding of fundamental interactions also governing the physics of inner-shell electrons in both neutral atoms and ions in low charge states. Isoelectronic sequences of all elements multiply the number of objects of

J. R. Crespo López-Urrutia (✉) · Z. Harman
Max-Planck-Institut für Kernphysik, Saupfercheckweg 1, 69117 Heidelberg, Germany
e-mail: crespojr@mpi-hd.mpg.de

Z. Harman
e-mail: z.harman@mpi-hd.mpg.de

W. Quint and M. Vogel (eds.), *Fundamental Physics in Particle Traps*,
Springer Tracts in Modern Physics 256, DOI: 10.1007/978-3-642-45201-7_10,

study available for experiments. Because of the different scaling laws of the various interactions, their relative strengths can be tuned along such series, providing a tool to disentangle their effects.

10.2 Quantum Electrodynamics Studies with Trapped HCI

Both quantum electrodynamics (QED) effects and relativistic contributions to the electron binding energies show a steep $\propto Z^4$ dependence on the atomic number Z. Another central scaling law of QED energy corrections is their $\propto 1/n^3$ dependence, with n being the principal quantum number. Therefore, electrons in deeper shells of heavy elements acquire the largest binding energy contributions. As a consequence, the perturbative treatment of QED, which is well suited for small QED corrections breaks down, as the series expansions in terms of α^n has to be extended to include terms in the form of $(Z\alpha)^n$ that do not rapidly converge at high charges and require a completely different mathematical treatment.

In principle, these points also apply to neutral atoms, as well as to ions in any charge state. But for spectroscopy it is crucial both to reduce the complexity of the system and to extend the lifetime of the states which have to be interrogated. Therefore, heavy atoms are less suitable for these studies, since their filled, neutral electronic shells introduce correlations effects that are difficult to disentangle from the QED contributions. Furthermore, their inner-shell excitations usually decay by fast Auger processes that broaden the energy spectrum of both the competing radiative decay and Auger electron energy. It thus seems logical to use ions of heavy elements with the lowest possible number of bound electrons, found in the hydrogen-like, the helium-like, and the lithium-like isoelectronic sequences. The simplicity of the first makes it ideal for the study of a bound two-body system. The second one constitutes the simplest example of a three-body system including two strongly correlated fermions. In the third one, a quasi one-electron system again, the calculable, reduced overlap of the electronic wave function with the nucleus allows for complementary investigations of QED and nuclear size (NS) effects. Important theoretical questions which have been experimentally investigated are the one-loop, two-loop, and screened (many-electron) QED contributions, the treatment of the negative energy spectrum of the bound electrons, of the Breit interaction, as well as the calculation of electron correlations using multi-configuration Dirac-Fock (MCDF), relativistic many-body perturbation theory (RMBPT), and relativistic configuration interaction (RCI) schemes. Effects arising from nuclear structure such as finite nuclear size (NS) effects, nuclear recoil, hyperfine interactions and their anomalies represent another very interesting field of research with HCI, which show extremely magnified contributions of these effects. An interesting summary of these issues and references to the relevant literature can be found in Refs. [1, 256].

10.3 Historical Development of Experiments with Electron Beam Ion Traps

Laboratory work with HCI requires practical sources of these species. From a spectroscopical point of view, a line-shaped radiation source of the highest possible density and at a very low temperature would seem ideal. For HCI sources, however, compromises are necessary, since HCI production encompasses tremendous concentration of energy in various forms upon the educt atoms in any given target ensemble. Thus, the product HCI will show high kinetic energies and temperatures. Stationary conditions can be difficult to achieve, as the presence of steep density as well as temperature gradients leads to a rapid expansion of the targets. The different mobilities of electrons and ions in a plasma also induces strong electromagnetic fields with a fast temporal evolution. Transient sources using electrical discharges or laser-produced plasmas suffer from these limitations.

Fortunately, these obstacles can effectively be circumvented since the introduction of the electron beam ion trap (EBIT). Its principle, ion production and trapping by a focused electron beam, quickly leads to a steady-state spatial distribution of HCI occupying a small cylindrical volume with a large aspect ratio [2, 3]. This arrangement is very well suited for coupling to spectroscopic equipment, as shown in Fig. 10.1. Mutual ion repulsion is compensated by the negative space charge potential of the electron beam, which is focused by a strong magnetic field overcoming its own tendency to expand. By virtue of the large mass difference between projectile electrons and atomic targets, momentum transfer is rather slow, and the heating proceeds by orders of magnitude less abruptly than in other HCI sources [4]. At the same time, ions of different charge states evaporate from the trapping potential at enormously disparate rates, and so some species can act as coolants for others. These advantages have been essential for the many applications of EBITs to spectroscopy of HCI. Starting from the X-ray region, where the first experiments took place, this chapter will visit all regions of the electromagnetic spectrum and present essential contributions of different groups to this field of research.

After the introduction of the electron beam ion source (EBIS) [5–7], it became obvious that production of HCI by means of focused electron beams was rather effective. However, EBIS could not generate the highest possible charge states. It was presumed that this was due to plasma instabilities heating up the trapped ions and reducing their interaction time with the beam. Moreover, the EBIS design did not offer adequate diagnostic ports for spectroscopic work. Both problems were overcome with the invention of the EBIT (see Fig. 10.1) by Levine and Marrs [2, 3, 8–11] at Lawrence Livermore National Laboratory (LLNL). By reducing the total length of the device and changing the electron beam design, a stable and more compressed beam was achieved, while the Helmholtz configuration of the superconducting coils introduced in the design granted optical access to the center of the region where the ions interact with the beam. At the same time, the beam was sufficiently stable to allow for long trapping times without ion losses by heating. It was soon realized how important evaporative cooling was to keep species of interest from leaving the trap,

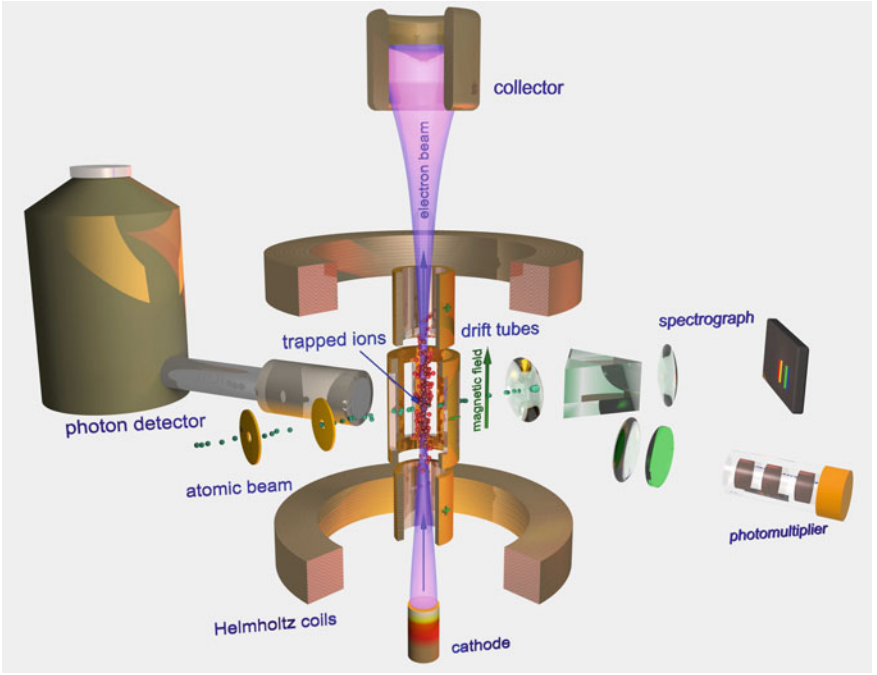

Fig. 10.1 Principle of an electron beam ion trap. Electrons emitted by a thermoionic cathode at the *bottom* are accelerated and launched into the magnetic field generated by the superconducting Helmholtz coils depicted. The Lorentz force acting on electrons counteracts their mutual repulsion and compresses the beam. As it passes through the central drift tube, the beam ionizes neutrals injected as an atomic beam (*left*), and traps the ions thereby produced by virtue of its negative space charge. Ion escape in the axial direction is suppressed by positive potentials applied to the drift tubes below and above of the central one. X-ray detectors or other spectrometers gain optical access to the trapped ion cloud through slotted apertures in the central drift tube

and careful modelling by Penetrante [4] pointed to the underlying principles of the time evolution of charge states and ion temperature, which were soon experimentally confirmed [12, 13].

From its introduction in the year 1986 on, EBITs have become the most useful instruments for the investigation of the properties of HCI. Their larger competitors, accelerators and ion storage rings, can indeed also perform very well, and even outperform EBITs in certain tasks, but the scope and variety of experimental techniques associated to EBITs is remarkable.

Initially, ion production was monitored in EBITs by X-ray photon detectors, soon complemented by crystal spectrometers. Later, the soft X-ray range was also covered by similar instruments and also grating-based devices. Optical spectrometers followed soon thereafter. With the inception of lifetime-measuring techniques [14] and the magnetic trapping mode [15], EBITs became an established tool for investigation of quantum processes in time scales spanning from the femtosecond range

of the fast X-ray transitions to the millisecond domain in which forbidden optical transitions take place, an amazing twelve orders of magnitude.

Particularly fruitful have been experiments utilizing the variable electron beam energy as a tool to resonantly excite inner-shell electrons by photo-recombination. As the time reversal of the Auger process, dielectronic recombination plays a crucial role in the temperature and ionization balance of hot astrophysical and laboratory plasmas, and in the opacity of stellar interiors.

Finally, a compact scientific tool was available for investigating the, in the Universe ubiquitous, HCI in the laboratory. Application of the novel device to fundamental studies started immediately at LLNL. Soon, the importance of the development became clear in the wider community, and other groups followed rapidly along the same path. Two EBITs based on the LLNL blueprint were built at Oxford University [16, 17] for that group and for the one based at the National Institute for Standards and Technology (NIST) [18, 19]. A device of the same design was purchased for the Max-Planck Institute for Plasma Physics subsidiary in Berlin from a company based in Livermore. In Japan, strong efforts led to the construction of another superconducting EBIT inspired by the Livermore model [20–22]. A French group around J. P. Briand developed a very compact electron beam ion trap using permanent magnet technology which showed very promising capabilities [23]. Meanwhile, strong scientific activity went on at the LLNL team and the younger then existing groups. Since the commissioning of the high energy SuperEBIT [2], even bare uranium ions, which hitherto had only been accessible at relativistic velocities in high-end accelerators, became available in a trap. Beiersdorfer has recompiled the history of those pioneering LLNL experiments until the year 2008 in a review paper [24].

The cross sections for the production of heavy hydrogen-like ions were determined by analyzing the beam geometry and the ion yield [25]. Lifetimes of excited levels in the fs range could be determined based on the natural line width of X-ray transitions [26]. With the magnetic trapping mode [15], it became possible to reduce the background caused by electron impact excitation (EIE) as well as bremsstrahlung in certain types of measurements, and also to suppress the quenching of metastable states allowing for precise lifetime measurements [14, 27–35]. A wide variety of experiments with HCI [36] had become possible, addressing important questions of QED in strong fields (for an introduction to these theoretical questions in the perspective of EBIT experiments see e.g., the short reviews by Cheng [37] and Sapirstein [1]).

By the end of the 1990s, in addition to the original vertical design, a horizontal type was introduced at the Freiburg University EBIT (FreEBIT) [38] to allow for more convenient ion extraction and for the use of commercially available superconducting magnet technology with much lower liquid helium consumption than the first devices. Plans were also drafted there for an EBIT geared towards investigations at free-electron lasers and synchrotrons, which later became FLASH-EBIT [39], and for another twin device with applications to charge breeding of short-lived isotopes, the TRIUMF-EBIT. Elsewhere, vertical EBITs were planned and came into operation in Shanghai [40] and Stockholm [41]. Commercial models achieving some of the performance of the cryogenic devices appeared on the market [42]. Quite recently,

small, compact EBITs used for visible and VUV emission spectroscopy have been introduced by the Tokyo and Shanghai EBIT groups [43, 44].

In recent years, laser spectroscopy with EBIT trapped ions has been applied to the study of the Lamb shift in hydrogen-like and lithium-like ions, of accurate wavelengths of coronal lines, to the QED contributions to the binding energy. Combination of EBITs with free-electron lasers [39] and synchrotron radiation sources [45–47] has resulted in the first examples of laser spectroscopy in the X-ray region [48, 49], with applications to both fundamental and applied physics. And the inherent stability of quantum states in HCI against external perturbations has lead to the first attempts for using trapped HCI to investigating the time variation of fundamental constants.

Given the large literature body which has originated from research with EBITs, we will have to restrict ourselves in this chapter to a partial view focused on a few experiments that aimed at simple electronic systems with few bound electrons, and exclude experiments with straightforward applications to the study of the electronic structure of complex ions. This latter field has also central position in atomic physics, since HCI are truly essential and abundant constituents of stars and astrophysical plasmas (for a review see Ref. [50]), such as those found in the powerhouses of active galactic nuclei, in accretion disks around black holes, and spectroscopic diagnostics are key for understanding the physics of such objects.

10.4 Production and Trapping of Highly Charged Ions by Electron Beams

HCI require energetic collisions for their production. The most efficient mechanism is electron impact ionization (EII), for which the cross sections at threshold are zero, and grow with the energy, peaking at approximately two and a half times the ionization potential. However, in presence of a trapping mechanism, the small cross section at threshold is compensated by the long interaction times.

As its name already states, an EBIT starts with an intense beam of electrons. Inside the trapping region (see Fig. 10.2), the electron beam is compressed by a strong magnetic field which produces a magnetic pressure keeping the beam from expanding due to the mutual repulsion of its particles. A very high density beam (reaching values of thousands of amperes per square centimeter) is the result, which induces a negative space charge potential arising from the 'line charge' (see Fig. 10.3). At typical operation parameters, the potential difference between the central axis of the electron beam and its boundary is of the order of tens to hundreds of volts. Across the distance to the inner wall of the central drift tube, the potential difference may reach kilovolt values [51].

Small EII cross sections call for the highest possible current density. Indeed, the electron beams realized at EBITs belong to the most intense examples available. Their ancestors were the ones used in travelling wave tubes and other microwave-generating devices. By perfecting electron beam injection into the EBIT and optimizing its

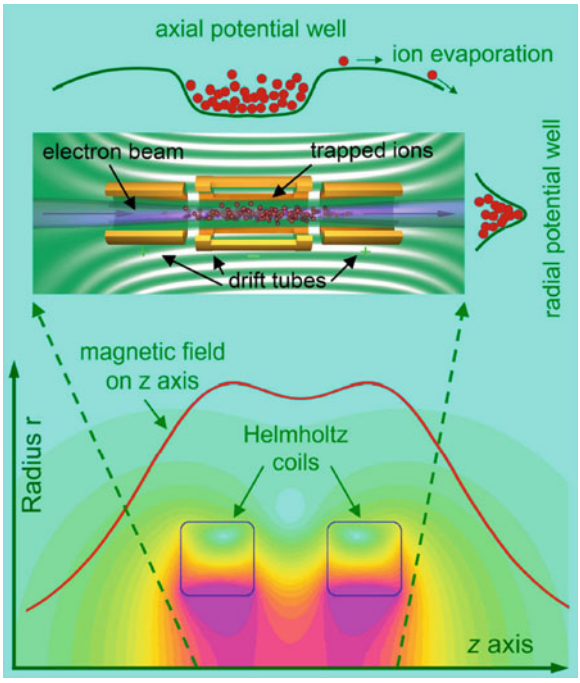

Fig. 10.2 Principle of operation of an electron beam ion trap. A strong magnetic field (value at axis given by *red curve*) generated by Helmholtz coils (*bottom*, false colour map) is used to compress an electron beam launched into its axis. The negative space charge potential (*top insert*) induced by the beam confines the motion of positive ions radially. Its value is sketched as a function of the separation from the axis (*top*, *right*). An axial electrostatic potential well (*top center*) produced by voltages applied to the drift tubes traps the ions axially. At a typical current of 200 mA, a potential difference of ≈200 V between the center and the edge of the electron beam (typical radius ≈70 μm) arises from the negative charge

transport with superconducting magnets, the currently achieved current area densities of more than 10^4 A/cm^2 imply that atoms are hit millions of times every second. With electron concentrations of 10^{13}/cm^3 at its center, the beam represents a 0.3-mbar pressure-equivalent concentration of negative charges, and also causes a nearly as dense positive ionic charge accumulation. All this occurs within an ultra-high vacuum environment which is roughly ten orders of magnitude thinner. It is here, at conditions rather similar to those prevailing in astrophysical plasmas widely found in stellar coronae, where the physics of ionization and recombination between these two classes of partners gives rise to a wide variety of processes that have to be understood in the first place. When a neutral atom or molecule moving at typical thermal velocities crosses the electron beam at the center drift tube (see Figs. 10.2 and 10.4), it is ionized with a high probability in a time scale of microseconds or less. The negative space charge potential then traps the resulting ion within the electron beam, and the repeated interactions with it strip more and more electrons from the

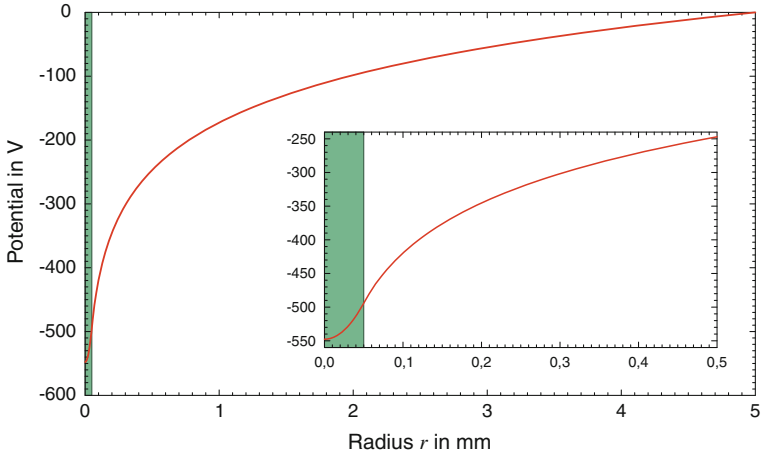

Fig. 10.3 Space charge potential generated by an electron beam as a function of the radial separation from the beam axis. The green shaded region indicates the beam radius. The insert shows a magnified view of the potential at a close distance from the electron beam. Even inside the beam itself, a potential difference of 50 V arises from the presence of the negative charges

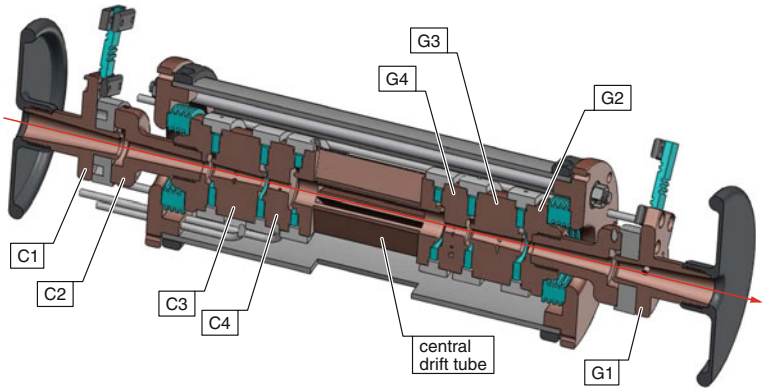

Fig. 10.4 Section through the trap electrodes, or drift tubes, of a cryogenic electron beam ion trap (FLASH EBIT [39]). Sapphire insulators are used to separate the different elements. Slotted apertures in the central electrode allow for viewing the ions trapped within it. The whole assembly is approximately 350 mm long,and the inner diameter of the drift tubes (labelled G1–G4, C1–G4, and the central one) varies from 5 to 15 mm

trapped ion. Although the cross sections for EII rapidly decrease with the removal of the external electronic shells, the trapping time amply compensates for their reduction. The average charge state of the ions rises in time, keeping a rather narrow distribution. This can be used to measure the cross sections for ion production, as, e.g., in the case of hydrogen-like ions [25, 52, 53]. Eventually, no more electrons can be stripped, when the binding energy of the remaining ones is higher than the kinetic

energy of the beam electrons. The choice of this energy is essential for the charge states being generated. However, a pure ensemble of ions in a single charge state is never fully achieved. Quite frequently, a continuous injection of neutrals as an atomic beam is used. In this case, a wide distribution of charge states results, since the interaction time of the trapped species with the beam varies [13, 54]. This effect is not present when pulsed injection of atoms or ions is applied. In cases where very heavy elements are injected and very high charge states are aimed at, the recombination processes (radiative and dielectronic recombination as well as charge exchange with residual gas) efficiently compete with EII. Then, due to ion-electron recombination, the charge state distribution encompasses also several charge states.

10.5 Physical Processes in the Trap Region

Whenever electrons and ions encounter, their collisions induce dynamic processes that are paramount for the energetics and composition of plasmas in general. First of all, EII drives the ion production. While the direct process can bring electrons into the continuum always at any projectile energy surpassing the binding forces, its cross section is quite often dwarfed by the one corresponding to indirect pathways following electron impact excitation of an inner-shell electron to an outer shell, and the subsequent collapse of the electronic shell with emission of Auger electrons.

At the same time, the reversibility of quantum processes at the atomic level leads to the appearance of radiative recombination (RR), the time reversal of photo-ionization. Here, photons are emitted instead of being absorbed, and their energy is larger than that of the projectile electron in the ionic reference frame. Once some of the electronic shells offers vacancies, electrons from deeper levels are continuously cycled in EIE and photonic as well as auto-ionization decay (AI). Again, the strong resonant time-reversed process, called dielectronic recombination (DR), competes with the up-charging mechanisms and generates strong emission lines. In both directions, electronic correlations have proven to be a key element for the dynamic evolution of the charge states.

Independently of the presence of free electrons, residual gas offers for HCI a potential reservoir for replenishment of the missing negative charges. In most EBITs, cryogenic pumping due to the cold surfaces at near 4 K lowers the pressure into the $\approx 10^{-13}$ mbar range, reducing the neutral particle density accordingly, and therefore strongly suppressing charge exchange. However, it is also possible to intentionally enhance charge exchange by injecting a dense atomic beam in a pulsed mode into the trap region [55]. Analogously to the situation in the atmospheres of planets and comets [56] under the effects of the solar wind, recombination of HCI by charge exchange produces not only ions in lower charge states but also recognizable X-ray spectral lines [15, 56] which can be used for plasma diagnostics or for a background-free study of resonance transitions.

The individual mechanisms driving the trap physics, but also governing the radiation balance of hot plasmas in astrophysics and tokamaks, are described in the following subsections.

10.5.1 Electron Impact Ionization

Under typical EBIT operating conditions, the current density in the beam reaches values of $10^{22}\, e/(\mathrm{s}\cdot\mathrm{cm}^2)$, the equivalent of several thousand amperes per square centimeter. For an atom with an assumed typical EII cross section of $10^{-16}\,\mathrm{cm}^2$, the initial ionization rates lie in the MHz range, much faster than all other processes. Thus, this process dominates the charge evolution within the trap region. When the kinetic energy of the impacting electron E_e is higher than the ionization potential I_p of the least-bound electron, its ejection can result with a given probability. Since energy is conserved,

$$A^{q+} + e^-(E_e) \rightarrow A^{(q+1)+} + e^-(E_1) + e^-(E_2) \quad \text{and} \quad E_e - I_p = E_1 + E_2. \tag{10.1}$$

Here, the notation A^{q+} stands for an ion of the element A with a net positive charge q. A rough estimate for the EII cross section can be obtained utilizing the semi-empirical formula given by Lotz [57]:

$$\sigma_i^L[cm^2] = 4.49 \times 10^{-14} \frac{N}{I_p^2} \frac{\ln(u+1)}{u+1}\,, \tag{10.2}$$

with $u = E_e/I_p - 1$ and N being the number of equivalent electrons in the same shell.

10.5.2 Electron Impact Excitation

After the initial ionization steps, the availability of open shells closer to the ground state gives rise to much stronger couplings between initial and the now possible, unoccupied final states by collisional interactions. Excitation at a given projectile electron kinetic energy E_e of the incident electron follows when this is higher than the energy difference from the level n to n'. The complete process, involving subsequent radiative decay of the excited state $\left[A^{q+}\right]^*$, can be represented as follows:

$$A^{q+} + e^- \rightarrow \left[A^{q+}\right]^* + e^- \rightarrow A^{q+} + \hbar\omega\,. \tag{10.3}$$

Here, $\hbar$ is the reduced Planck constant, and ω is the angular frequency of the emitted photon. For the case of resonant excitation resulting in a hole state:

$$A^{q+} + e^- \rightarrow \left[A^{(q-1)+}\right]^{**}, \tag{10.4}$$

and relaxation can proceed either through auto-ionization following the scheme $\rightarrow \left[A^{q+}\right]^{*} + e^-$ or by photon emission $\rightarrow A^{(q-1)+} + \hbar\omega$. Already for ions in moderately charged states, the rates for photon emission compete and overcome the typical Auger rates, which are rather independent of the charge state.

An useful approximation for the excitation cross sections is represented for an electric dipole transition with an energy $E_{n,n'}$ by the Bethe formula [58]:

$$\sigma_{ex} \approx \frac{A}{E_e} + B\frac{\ln E_e}{E_e}, \quad E_e \gg E_{n,n'}, \tag{10.5}$$

where A is a constant, and the parameter B is linked to the corresponding oscillator strength. Basically, this results from the fact that electronic collisions can be seen as a pulse of virtual photons coupling with the bound electrons through dipole–dipole interaction. This connection is applied in the empirical Van Regemorter formula [59] for calculation of electric dipole-allowed cross sections:

$$\sigma_{ex}^{\mathrm{VR}}(x)[cm^2] = 2.36 \times 10^{-13}\frac{1}{E_{n,n'}^{2}}\frac{G(x)}{x}f_{n,n'}, \tag{10.6}$$

where the dimensionless parameter x is defined for a given transition $n \rightarrow n'$ as the ratio between the kinetic energy of the incoming electron and the threshold energy $E_{n,n'}$: $x = E_e/E_{n,n'}$. The value $f_{n,n'}$ is the photon absorption oscillator strength. The term $G(x)$ is called the effective Gaunt factor, which scales the classical oscillator strength to that of a quantum mechanical system. Van Regemorter [59] uses for this factor another empirical approximation as

$$G(x) = 0.349\ \ln(x) + 0.0988 + 0.455\, x^{-1}. \tag{10.7}$$

10.5.3 Radiative Recombination

When an ion captures a free electron under emission of a photon, and lowering its charge state by one,

$$A^{q+} + e^- \rightarrow A^{(q-1)} + \hbar\omega_{RR}\,, \tag{10.8}$$

energy conservation requires that the photon energy be equal to the sum of the kinetic energy of the projectile and the binding energy of the ion in the final state. The condition is stated as:

$$\hbar\omega_{\mathrm{RR}} = E_e + I_p. \tag{10.9}$$

In order to obtain the energy-differential RR cross section, one can apply the principle of detailed balance to the photo-ionization cross sections (σ_{ph}):

$$g_q \sigma_{\mathrm{ph}}(\omega) = \frac{2m_e c^2 E_e}{\hbar^2 \omega^2} g_{q+1} \sigma_{\mathrm{RR}}(E_e), \tag{10.10}$$

where the statistical weights for each principal quantum number n are given by $g_q = 2n^2$ for the final state and $g_{q+1} = 1$ for the initial one. σ_{ph} can be estimated by means of the Bethe and Salpeter formula [60]. Kramers obtained for the RR cross section the following expression:

$$\sigma_{\mathrm{RR}}^{\mathrm{Kramers}} = \frac{32\pi a_0^2 \alpha^3}{3\sqrt{3}} \frac{Z|E_0|^{3/2}}{(E_0 + E_e)\, E_e}, \qquad E_0 = Z^2 Ry/n^2. \tag{10.11}$$

In order to obtain more accurate values, the use of advanced atomic structure methods and computer codes is required. Useful modules for calculating RR and photo-ionization cross sections are part of the Flexible Atomic Code by Gu [61] and the RATIP package by Fritzsche [62].

10.5.4 Dielectronic Recombination

In dielectronic recombination, the free electron is captured into a vacant excited state of the ion A^{q+} transferring non-radiatively the energy difference to a core electron with energy E_1, which is simultaneously promoted to a higher-laying excited state with energy E_2 of the ion, thus forming an intermediate (singly, doubly or multiply excited) state, as shown on Fig. 10.5. This step is then followed by the emission of a photon (or several photons):

$$A^{q+} + e^- \rightarrow \left[A^{(q-1)+}\right]^* \rightarrow \left[A^{(q-1)+}\right] + \hbar\omega_{DR}. \tag{10.12}$$

This resonant process can only happen when the energy difference between the core electron state and the state in which the second electron is excited is equal to the kinetic energy of the free electron E_e plus the binding energy I_p of the recombined state. This resonance condition is written as

$$\Delta E = E_2 - E_1 = E_e + I_p\,. \tag{10.13}$$

In the second step, the formed excited state $\left[A^{(q-1)+}\right]^*$ may as well decay to the ground state via an Auger auto-ionization process, where again there is a change in the ion charge as the ion returns to its initial state. However, in HCI, radiative de-excitation via emission of one or more photons strongly dominates. While the Auger rates are proportional to the electron–electron interaction and show only a

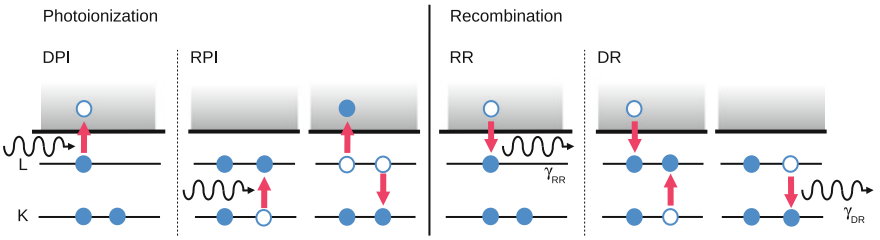

Fig. 10.5 Photo-ionization (*PI*) can proceed both directly (*DPI*) and resonantly (*RPI*). On the *right side*, the time-reversed processes, namely, radiative recombination (*RR*) and dielectronic recombination (*DR*) are depicted [63]

weak dependence on Z, the radiative decay rates increase with Z^4 for dipole-allowed transitions, and with up to very high powers of Z for magnetic, two-photon or higher-order transitions. In this way, radiative stabilization of the excited intermediate states is usually the dominant channel in HCI, in contrast to neutrals, where Auger processes dominate.

Dielectronic recombination is the time-reversed Auger process and, thus, the corresponding pathways are labelled accordingly. For instance, in a KLL DR resonance for a helium-like initial state, as shown in Fig. 10.5, the free electron is captured into the L shell of an ion, while a bound electron is promoted from the K shell to the L shell to form an excited $1s2l2l'$ state (with l, l' denoting single-electron angular momentum states). This intermediate excited state decays radiatively:

$$\begin{aligned} e^- + A^{(Z-2)+}\ (1s^2) &\rightarrow \left[A^{(Z-3)+}\right]^*\ (1s2l2l') \\ &\rightarrow A^{(Z-3)+}\ (1s^2 2l \text{ or } 1s^2 2l') + \hbar\omega(K_\alpha). \end{aligned} \tag{10.14}$$

To a good approximation, the energy dependence of the cross section of resonant recombination is described by a Lorentzian peak. The magnitude of the process is best characterized by the area of the resonance peak, which is customarily named resonance strength. Cross sections and resonance strengths for DR will be discussed later in Sect. 10.7.1.

10.6 Photon Spectroscopy Under Electron Beam Excitation

The first observations of ions trapped in an EBIT were carried out using solid-state photon detectors to analyze their X-ray emission upon EIE, generating characteristic bound–bound radiation. Furthermore, radiative recombination of mono-energetic electrons into open shells produces narrow transitions which immediately reveal the principal quantum number of the vacancies into which the electrons are captured. An example of a recorded photon emission spectrum is given in Fig. 10.6. Far higher

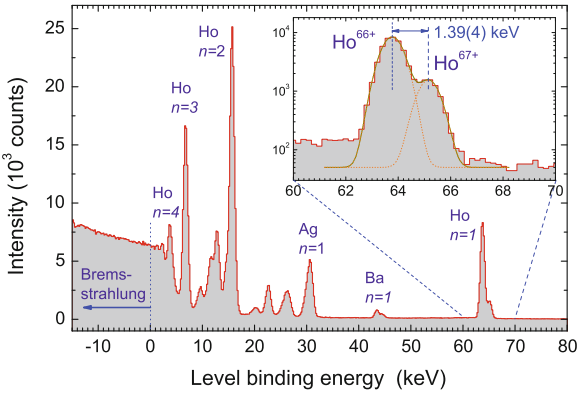

Fig. 10.6 X-ray photon spectrum of trapped holmium ions under excitation by an electron beam with an energy of 132.7 keV. This value has been subtracted from the photon energy to display the energy additionally liberated during radiative recombination (*RR*) into the different open shells (see labels) of the trapped holmium ions, which corresponds to the binding energy of the corresponding level. *Insert* RR peak of the $n = 1$ shell. The only vacancies in this shell occur in the cases of the bare Ho^{67+} ion and of hydrogen-like Ho^{66+} ions. The emitted photons have an energy difference (*indicated*) equal to the two-electron contribution to the binding energy

spectral resolution was soon reached at LLNL [64] by using crystal spectrometers of various kinds [65, 66]. A distinct advantage of the EBIT as a radiation source is the narrow confinement of the emitting particles in a narrow cylindrical volume with a diameter on the order of 100 µm [51], which constitutes the geometric equivalent of an entrance slit for the spectrometer. With the introduction of appropriate grating instruments, spectroscopy in the soft X-ray and vacuum ultraviolet region also became possible [67–73]. The more recent introduction of X-ray micro-calorimeters at EBITs (see e.g. [56, 74]) offers simultaneous spectral coverage over much wider regions than it is possible with crystal spectrometers, while achieving a much higher resolving power than typical solid-state photon detectors.

10.6.1 The X-ray Region: Lyman-α Transitions of Hydrogen-Like Ions

The Lyman-α lines of hydrogenic ions are the touchstone of atomic structure theory. Due to the comparatively simple structure of such single-electron systems, bound-state QED allows an accurate prediction of transition energies. Within relativistic quantum mechanics, the energy levels of hydrogenic ions are given by the Sommerfeld formula. Radiative corrections beyond the Dirac theory are described by self-energy diagrams, representing the energy shift of the bound electron due to its interaction with the vacuum fluctuations of the electromagnetic field, and by vacuum polarization diagrams, which depict the virtual creation and annihilation of electron–positron pairs in the field of the nucleus. These diagrams on the one-loop level

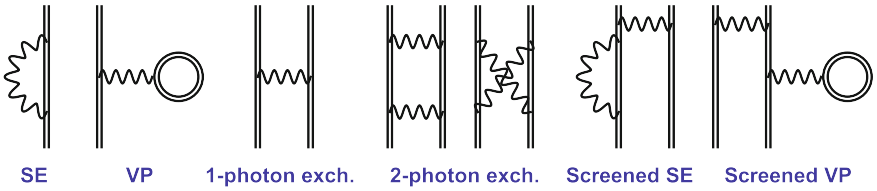

Fig. 10.7 Furry-picture [84] Feynman diagrams representing: (*left*) one-loop self-energy (*SE*) and vacuum polarization (*VP*) corrections to the energy levels in hydrogenic ions; (*center*) exchange diagrams with one and two photons in many-electron ions; and (*right*) two typical QED screening diagrams in many-electron systems. The *double lines* indicate wave functions and propagators for the electrons moving in the Coulomb field of the nucleus, and *wavy lines* depict virtual photons

(i.e. in first order in α (fine-structure constant) expansion) are shown on the left side of Fig. 10.7. In light hydrogenic ions, these corrections can be evaluated to a large extent analytically by employing truncated expansions in powers of the interaction strength $Z\alpha$ (see e.g. [75, 76]). In highly charged ions, such an approach fails as $Z\alpha$ cannot be regarded as a small parameter, and a theoretical ansatz is called for which treats the interaction with the nucleus in an all-order fashion. The calculation of one-loop QED corrections in all order in $Z\alpha$ has started decades ago and has been refined over the course of time [77–84]. Due to their comparatively high accuracy, theoretical transition energies of hydrogen-like ions, as for instance given in the tables by Johnson and Soff [79], are often simply taken as calibration standards [85, 86].

The improvement of experimental techniques with regard to accuracy and the accessible range of nuclear charges necessitated the calculation of two-loop QED corrections (see e.g. the work of Yerokhin, Indelicato and Shabaev [87]). Besides QED terms, calculations also have to account for effects arising from finite nuclear size [82, 88] and mass [84, 89, 90]. In inner-shell transitions of heavy ions, the polarization of the structured nucleus by the field of the orbiting electron gives rise to further small level shifts [91]. Figure 10.8 shows the dependence of the different contributions on the atomic number Z and compares one-loop and two-loop corrections and nuclear-size effects. Reviews by Mohr, Plunien and Soff [82], Shabaev [84] and Cheng et al. [256] summarize the progress of high-precision QED calculations in highly charged ions.

Early experimental work with HCI by Briand et al. at the Bevalac accelerator facility was dedicated to hydrogen-like Ar^{17+} and Fe^{25+} [92, 93]. Källne et al. and Richard et al. measured Cl^{16+} [94, 95], Tavernier at al. [96] hydrogenic Kr^{35+}, and Marmar determined the Lamb shift of the Ar^{17+} ion [97]. At GSI, Deslattes and Beyer studied the Lamb shift in hydrogen-like Ar^{17+} [98, 99] and Ni^{27+} [100] by observing the radiative decay of recoil ions in the charge state that had been produced by energetic collisions with relativistic heavy ions [101].

Independently of wavelength measurements calibrated with emission lines from solid targets excited by electron impact, for which various systematic effects are present, there has been a small number of absolute energy determinations based on crystallographic standards. Beiersdorfer carried out EBIT investigations of the

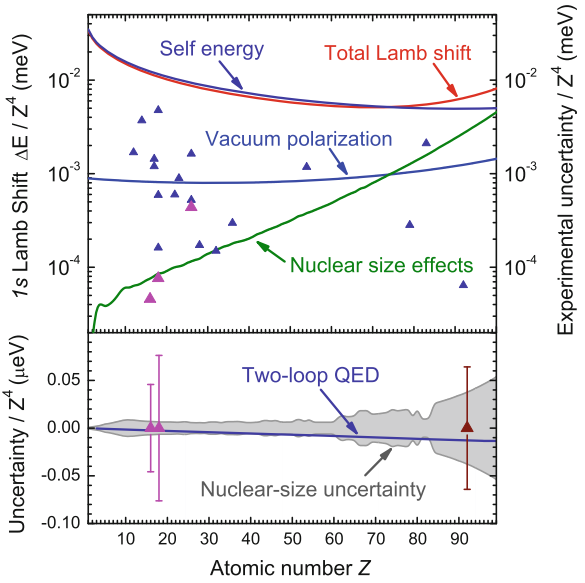

Fig. 10.8 *Top* scaling of one-loop QED contributions (self-energy, vacuum polarization) and nuclear-size effects as a function of the atomic number Z for hydrogen-like ions according to Johnson and Soff [79]. *Bottom* Comparison of the current uncertainty level due to nuclear-size effects (*grey shaded area*) with reported experimental uncertainties (*triangles*) for the measurement of the total Lamb shift in hydrogen-like ions and with the predicted magnitude of two-loop QED contributions to the binding energy (*blue curve*). For heavy elements, nuclear-size effects currently preclude a direct determination of two-loop QED corrections based solely on measurements of the hydrogen-like Lyman-α transitions. All energy values have been normalized by a factor $1/Z^4$ accounting for the first-order scaling of one-electron QED

wavelength of the two Lyman-α transitions in Mg^{11+} [102] using a quasi-monolith [103] with two crystal mounted in parallel which had been metrologically characterized. The two reflections from each line appear separated by a distance which allows determining the Bragg angle solely based on the crystal separation. An absolute value for the transition energy resulted with an error bar of 24 ppm. In order to infer the Lamb shift, the Dirac energy is simply calculated and subtracted from the experimental result. In the case of Mg^{11+}, this yields 0.246(44) and 0.351(70) eV for the Lamb shift correction to Lyman-α 1 and Lyman-α 2, respectively. For Si^{13+}, the value obtained in similar measurement had a larger error bar of 70 ppm [104].

Gillaspy et al. [105] measured at the NIST EBIT the energies for Lyman-α_1 ($1s-2p_{3/2}$) and Lyman-α_2 ($1s-2p_{1/2}$) in hydrogen-like V^{22+} to be 5443.95(25) and 5431.10(25) eV, respectively, in fair agreement with the theoretical values 5443.63 and 5430.70 eV. Nakamura and et al. [106] observed the intensity ratio between the two Lyman$_\alpha$ transitions in hydrogenic Ti^{21+} at the Tokyo EBIT. The Oxford group utilized a Johann crystal spectrometer [66] calibrated using the Kα lines of neutral vanadium [107] for investigating the 1s Lamb shift of hydrogen-like Ti^{21+}. Their determination yielded a value of 2.29(14) eV, in good agreement with the predictions (Fig. 10.9).

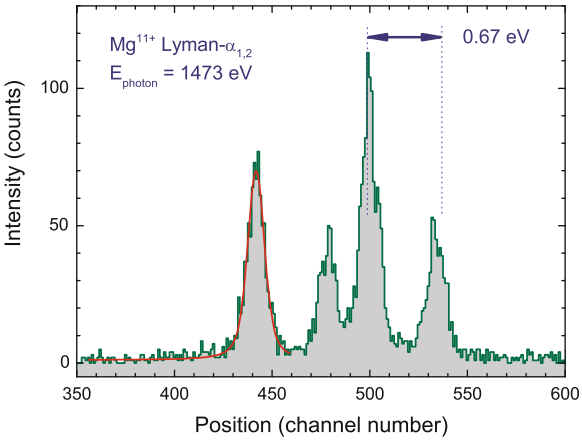

Fig. 10.9 High-resolution spectrum of the Lyman-α transitions of hydrogen-like Mg^{11+} [102] using a quasi-monolith consisting of two crystals mounted in parallel. Due to this arrangement, every line appears twice, showing a geometric splitting which is used for an absolute energy determination. The experimental resolution $E/\Delta E$ of nearly 9,000 already allows to separate the Lorentz natural line width ($\tau \approx 77$ fs) from the thermal broadening contribution in a Voigt fit

A recent approach to absolute transition energy measurements has been the application of the Bond method [108] to EBIT spectroscopy. In this technique, a flat crystal is turned from one Bragg reflection of the line of interest to the mirror symmetric reflection. By using two detectors and measuring the angle difference, the absolute Bragg angle can be obtained without offset correction. Since the lattice constant of silicon [109] is a secondary representation of the meter in the International System of Units (SI), the Bragg angle yields the wavelength, and thus the transition energy without the need for calibration lines. Bruhns et al. [110–114] implemented this method, which was later improved by Kubiček et al. [115–117] by including two laser beams as angular fiducials into the geometric scheme. By locating the source of the laser beams virtually at the position of the emitting ions within the trap region, the angular fiducials allowed to determine the X-ray position on the X-ray CCD detectors without needing to know the relative positions of source, crystal, or detectors. All the rays emanating from the X-ray source are reflected by the crystal which becomes a symmetry plane, and then they intersect the detector camera. The ratios of the respective separations between each fiducial and the X-ray line on the detector plane are in this configuration independent from the total distance between origin and detector. This setup eliminates the major sources of uncertainty typically found in Bond method determinations, while allowing to dispense with using slits to fix the incidence direction of the X rays, an approach which reduces the available intensity. With this technique, systematic measurements of the Lyman-α transitions in S^{15+}, Ar^{17+}, and Fe^{25+} were performed (see Fig. 10.10 and Table 10.1). The final uncertainty for S^{15+} reached a level of 1.4 ppm, not yet sufficiently small to allow for benchmarking predictions of two-loop QED contributions at this value of Z.

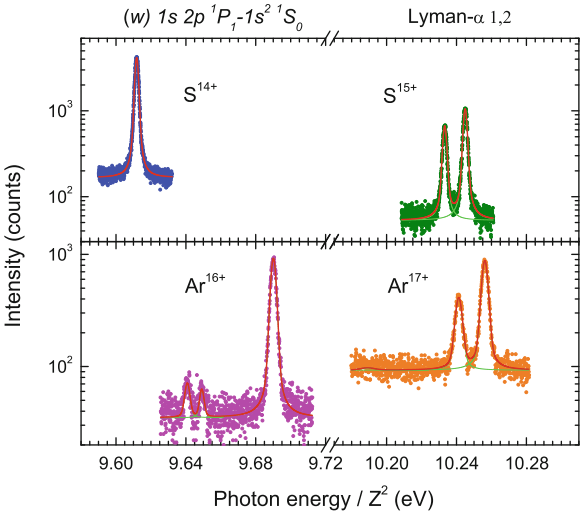

Fig. 10.10 Resonance transitions $2p \rightarrow 1s$ in helium-like (*left*) and hydrogen-like (*right*) sulphur and argon ions as observed in high-precision crystal spectrometer measurements [115–117]. The photon energies have been scaled by $1/Z^2$ in order to represent them in a common plot. This scaling removes the first-order Coulomb term from the transition energy and shows shifts due to correlation, relativistic and QED terms. The $1s2p\,^1P_1 \rightarrow 1s^2\,^1S_0$ shows a larger shift than the Lyman-α transitions due to interelectronic correlations, which are not present in the hydrogen-like system

Table 10.1 Experimental energies ($E_{exp.}$) for the Ly-α_1 and w ($1s^2\,^1S_0 \rightarrow 1s\,2p\,^1P_1$) transitions and inferred values for the $1s$ ground-state Lamb shift (LS) obtained at the Heidelberg EBIT [115, 117] compared with earlier measurements [99, 116, 135, 138, 139] ($E_{prev.\ exp.}$), unpublished data for Fe^{24+} from Rudolph [140] obtained with FLASH EBIT, and predictions ($E_{theo.}$) from references [141] (H-like),[124] (UM), [118] (all order in $1/Z$), [131] (BSQED)

Transition	$E_{exp.}$ (eV)	$E_{prev.\ exp.}$ (eV)	References	$E_{theo.}$ (eV)	References
Ly-α_1 S^{15+}	2622.693(3)			2622.6995(1)	[141]
LS S^{15+}	0.828(3)			0.8212(1)	[141]
Ly-α_1 Ar^{17+}	3322.993(8)	3322.989(17)	[99]	3322.9929(1)	[141]
LS Ar^{17+}	1.201(8)			1.2009(1)	[141]
Ly-α_1 Fe^{25+}	6973.18(66)	6972.732(609)	[139]	6973.1804(8)	[141]
LS Fe^{25+}	4.06(66)			4.0574(8)	[141]
w S^{14+}	2460.627(3)	2460.641(32)	[116]	2460.626(1)	[124]
				2460.629	[118]
				2460.6292(3)	[131]
w Ar^{16+}	3139.581(5)	3139.583(6)	[138]	3139.576(2)	[124]
				3139.581	[118]
				3139.5821(4)	[131]
w Fe^{24+}	6700.442(23)	6700.725(201)	[135]	6700.401(7)	[124]
		6700.513(80)	[140]	6700.424	[118]
				6700.4347(12)	[131]

10.6.2 The Heliumlike Sequence: A Test for Interelectronic Correlation

In many-electron ions, correlation effects increase the complexity of the theoretical description. Helium-like ions with their two electrons represent an archetype many-body system, therefore, a large literature list of theoretical work exists for the electronic structure of such ions.

Most atomic structure methods use the Hartree-Fock (HF) approximation, or, its relativistic generalization, the Dirac-Hartree-Fock (DHF) approximation as their starting ground. Here, the two-electron wave function is represented by an antisymmetrized product of single-electron orbital functions, i.e. the particles are assumed to be independent. Correlation contributions, defined as electron–electron interaction effects beyond the (D)HF approximation, can be either treated perturbatively or variationally.

The former approach is generally referred to as relativistic many-body perturbation theory (RMBPT). Plante, Johnson and Sapirstein carried out RMBPT calculations for helium-like ions, with corrections taken into account to all orders (AO method, Ref. [118]). In variational calculations, typically, a multiconfiguration approach is employed: the many-electron wave function $\Psi(JP)$ is represented as linear combination of Slater determinants $\Phi(JP)$ coupled to a given total angular momentum quantum number J and possessing a given parity P:

$$\Psi(JP) = \sum_{i=1}^{n_c} c_i \Phi_i(JP)\,. \tag{10.15}$$

Here, n_c is the number of configurations taken into account. In case of the multiconfiguration Dirac-Fock (MCDF) method, all single-electron orbitals used to construct the configuration state functions $\Phi(JP)$ are variationally optimized [119]. MCDF calculations for heliumlike ions were performed by Indelicato, with the inclusion of additional radiative corrections [120, 121]. In case of the relativistic configuration interaction method (RCI), the total Hamiltonian is diagonalized by using a fixed set of single-electron orbitals. Such calculations for two-electron ions were performed by Cheng et al. [122, 123, 256]. Both MCDF and RCI essentially include electronic correlations in all orders.

In a completely different approach, non-relativistic explicitly correlated wave functions are used, and relativistic and QED corrections are calculated perturbatively with these. This unified method (UM) of Drake [124–126] is rather successful since it is able to predict the dominant electronic correlation contributions better than earlier works.

Especially in heavy two-electron ions, a quantum electrodynamic treatment of electron interaction effects is mandatory. Here, the interelectronic interaction is described to lowest order in $1/Z$ by the one-photon exchange diagram (see Fig. 10.7), which, unlike the instantaneous Coulomb interaction, takes into account magnetic and retardation corrections. The QED expansion is further improved by taking into

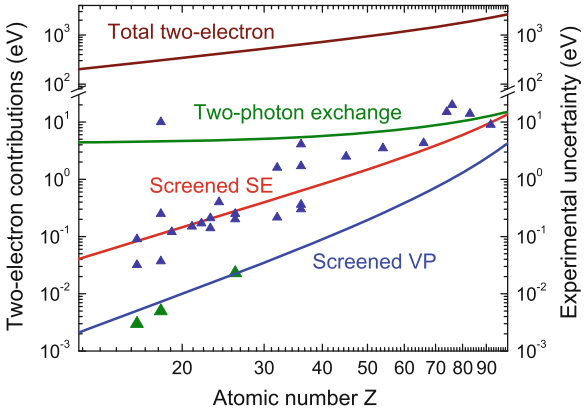

Fig. 10.11 Break-up of the absolute values of the different contributions to the binding energy of the $1s^2\,{}^1S_0$ ground state along the helium-like isoelectronic sequence resulting from electron–electron correlations and QED. The curves follow calculations by Artemyev [131]. The experimental uncertainties of different measurements are indicated as triangles for comparison. Recent work [115–117] (*green triangles*) allows to test screened vacuum polarization predictions

account two-photon exchange contributions (Fig. 10.7). Lindgren performed detailed QED calculations for the helium-like isoelectronic sequence [127, 128]. Essential aspects of the QED treatment, like the use of the no-pair Hamiltonian, the role of negative energy states are covered in the work of Johnson et al. [129] and by Sapirstein [130].

The exchange of virtual photons between the bound electrons also modifies the QED effects. Such corrections are described by the QED screening diagrams, containing both a SE or VP loop as well as an exchange photon connecting different electrons. Examples of such Feynman diagrams can be seen on Fig. 10.7. The most advanced QED predictions, containing results for QED screening, two-photon exchange as well as higher-order correlation effects were carried out by Artemyev and colleagues [131, 132]. Figure 10.11 shows the magnitude of the different physical contributions along the isoelectronic sequence.

Experiments in the range from $Z = 16$ to 39 were reported by Schleinkofer [133], Aglitsky [134] and Beiersdorfer [135] based on tokamak observations. They were based on plasmas with very high excitation rates, and contamination by satellite lines could sometimes have compromised the accuracy of those results. Alternatively, and for the same reasons, the helium-like lines and their satellites can be used for plasma diagnostic purposes, and Biedermann carried out experiments at the Berlin EBIT to that end [136]. The helium-like spectrum of argon [107] and vanadium [137] were also obtained.

Kubiček [115–117] determined with very small uncertainty absolute Bragg angles also for several helium-like electronic transitions. These latest measurements with improved resolution confirmed bound-state QED predictions by Artemyev et al. [131]. These results for He-like and H-like ions, together with earlier measurements

and theoretical predictions, are summarized in Table 10.1. Here, for completeness, we also introduce a result for helium-like iron from synchrotron radiation measurements (see Sect. 10.8.2).

10.6.3 The QED-Sensitive $2s_{1/2} \rightarrow 2p_{3/2,1/2}$ Transitions in Lithiumlike Ions

In this section, we focus on results obtained using trapped ions. For measurements of the $2s_{1/2} \rightarrow 2p_{3/2,1/2}$ transitions in lithium-like heavy ions using storage rings, we refer to the the work at GSI [142–146] and references therein.

Studies on the Lamb shift of U ions form U^{82+} to U^{89+} were carried out at LLNL by Beiersdorfer et al. already in 1993 [147]. A value of -47.39 ± 0.35 eV has been determined for the $2s$ Lamb shift, in agreement with the theoretical result of -47.58 eV by Blundell [148], based on the evaluation of radiative corrections with an approximate potential describing the screening of the $2s$ and $2p$ electrons by the $1s^2$ core. A value of 4025.23 ± 0.14 eV was found for the $2s_{1/2} - 2p_{3/2}$ transition in lithium-like Th^{87+} [149]. This value was sensitive to the effect of nuclear polarization and confirmed predictions of a 36-eV QED contribution to within 0.4 %. A similar test of QED and atomic structure calculations was also performed by measuring twelve $2s_{1/2} - 2p_{3/2}$ transitions in the neighbouring charge states. The measured transition energies in beryllium-like Th^{86+} through neonlike Th^{80+} were compared with theoretical predictions from MCDF calculations of the electron-correlation terms.

By means of a high resolution crystal spectrometer, Beiersdorfer et al. measured the $2s_{1/2} - 2p_{3/2}$ line in $^{209}Bi^{80+}$ [150]. Due to the large nuclear magnetic moment, a sizable hyperfine splitting of 0.820 ± 0.026 eV appears between the states $F = 4, 5$ in the $1s^2\,2s_{1/2}$ ground configuration, as shown in Fig. 10.12. The measurement had a very high accuracy due to its careful calibration with hydrogen-like transitions. Its averaged result of 2788.139 ± 0.039 eV for the transition constituted at that time an essential test of QED correction terms and motivated the evaluation of two-loop QED corrections for heavy elements [150].

For the lithium-like ion W^{71+}, Podpaly et al. determined a value of 1697.34 ± 1.03 eV for the $1s^2\,2s_{1/2}(J = 1/2) \rightarrow 1s^2\,2p_{3/2}(J = 3/2)$ transition using a flat crystal spectrometer [151]. This result is in agreement with the multiconfiguration Dirac-Fock prediction of 1696.0 eV by Kim et al. [152] and the configuration interaction value of 1697.6 eV [151]. However, the error bars were still rather large for rigorously testing QED corrections. Besides the lithium-like one, a range of charge states of tungsten was investigated, with applications to the diagnostics of fusion plasmas [151].

Beiersdorfer determined the two-loop contributions to the binding energy of the $1s_{1/2}$ electron [153] by scaling the nuclear-size contributions from lithium-like U^{89+} [154] to hydrogen-like U^{91+}. This inferred value is in perfect agreement with the theoretical prediction of Yerokhin et al. [87]. As for the transition energy of the

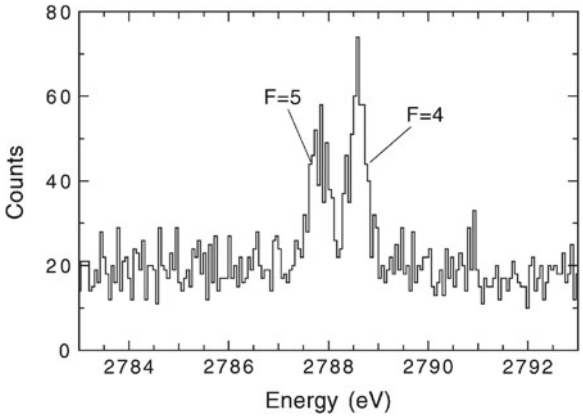

Fig. 10.12 X-ray spectrum of the $2s_{1/2} \rightarrow 2p_{3/2}$ transition in lithium-like $^{209}Bi^{80+}$ showing the two components due to the $F = 4$ and $F = 5$ hyperfine levels present in the ground state [150]. A very high resolution crystal spectrometer and efficient evaporative cooling were essential for this result obtained using SuperEBIT operating at 100 keV beam energy

lithium-like charge state, also a good agreement with bound-state QED predictions has been found [155]. Analogous experimental studies on the $3s$ electron QED shifts were performed for the $3s_{1/2} - 3p_{3/2}$ resonance line in sodium-like U^{81+} [156].

More recently, the energy of the $1s^2\,2p_{3/2} \rightarrow 1s^2\,2s_{1/2}$ transition in Pb^{79+} was measured with different isotopes at the Tokyo electron beam ion trap by Zhang et al. [157]. Due to its nuclear spin (I = 1/2), the transition in ^{207}Pb shows three blended hyperfine components. The transition energy result of 2642.260 ± 0.100 eV yields a QED contribution of 24.990 ± 0.100 eV which was compared with different calculations. The predicted isotopic shifts relative to ^{208}Pb are 0.1034, 0.0516, and 0.0258 eV for ^{204,206,207}Pb, respectively.

10.6.4 Spectroscopy of Forbidden Transitions in the Visible Range

Spectroscopic experiments determining optical transition wavelengths and lifetimes of few-electron ions represent a continuing challenge for the theoretical understanding, due to the complex interplay of electron correlation, relativistic, and QED effects. In the region of intermediate atomic numbers, these effects have comparable magnitudes (as measured, i.e., by their contribution to binding energies) and are intertwined. Measurements of lifetimes are especially informative in benchmarking structure theories since the radiative transition matrix elements are particularly sensitive to the long-range behaviour of the electronic probability density. Furthermore, experimental investigations of optical isotope shifts benefit from an increased sensitivity of HCI to effects arising from nuclear properties. Therefore, experimental

mass shifts in these systems provide on an ideal testing ground of relativistic nuclear recoil effects.

The first forbidden transition in an EBIT was observed by Morgan at the NIST EBIT. He detected the emission from the line connecting two low-lying states of the $3d^4$ configuration in titanium-like Ba^{34+} [158]. Later, Porto et al. continued these observations [159] along the isoelectronic sequence in ytterbium, tungsten and bismuth. Studies on the forbidden lines of Ba and Kr ions followed [27, 160]. Watanabe performed a systematic study of the M1 transitions in the titanium-like sequence [161] at the Tokyo EBIT. Other studies in this isoelectronic sequence are found in Ref. [162]. Bieber studied coronal lines in argon and barium ions at the Oxford EBIT [17]. Several measurements were performed at LLNL by Crespo et al. [163, 164]. Draganič [165] carried out very precise wavelength measurements in $Ar^{13+,14+}$ and Ba^{34+} and was able to resolve the Zeeman splitting of the transitions due to the magnetic field of the EBITs in Freiburg and Heidelberg. Soria Orts continued these investigations. An interesting outcome was her experimental confirmation [166] of relativistic mass shifts [89, 167], and also the determination of the g factor on the same ion [168]. An overview on the development of the field of visible transitions in HCI is given in [169].

Lifetime measurements of the $1s^2 2s^2 2p\ ^2P_{3/2}$ level of boron-like Ar^{13+} were performed [31, 170] at the Heidelberg EBIT [171]. The electron beam was switched on periodically to excite the trapped ions to the $^2P_{3/2}$ state and, then, switched off to detect the M1 decay to the ground state. Lifetimes were determined by recording the decay curve, i.e. the decrease of fluorescence intensity versus time. The experimental result of $\tau = 9.573(4)(5)$ ms (stat)(syst) agrees well with measured data of 9.70(15) ms [32], while being by more than an order of magnitude more accurate than previous experiments [32, 172–174]. Figure 10.13 displays a comparison with various theoretical and experimental results. The most recent calculation using the configuration interaction Dirac–Fock–Sturmian method (CI–DFS, Ref. [175]) yields a lifetime value $\tau = 9.538$ ms. The transition rate (Einstein coefficient) is proportional to the third power of the transition frequency. The corresponding wavelength has been accurately measured in Ref. [165], resulting in $\lambda = 441.2559(1)$ nm. In Fig. 10.13, theoretical results are displayed in different ways: (i) as published, (ii) corrected for the more accurate experimental transition frequency, and (iii) excluding and (iv) including the effect of the leading radiative correction in the electron anomalous magnetic moment (EAMM) approximation. The EAMM correction leads to a decrease of the lifetime by a factor $1 - 2\,\alpha/\pi$. Calculated lifetimes appear to cluster around a value of 9.53 ms, which is within a 3-σ disagreement with the experimental value. The reason of this discrepancy is not yet understood, triggering further theoretical calculations [176] and measurements with different ions and transitions to get to the root of this issue.

By means of a similar emission spectroscopy technique, the isotope shift of the above transition in Ar^{13+} and that of the $1s^2\,2s\,2p\,^3P_1$–$^3P_2$ line in Ar^{14+} was studied by measuring and comparing the wavelengths with the isotopes ^{36}Ar and ^{40}Ar. The isotope shifts were determined based on the wavelength differences, which had a sub-ppm accuracy. The details of the measurement can be found in Refs. [166, 183].

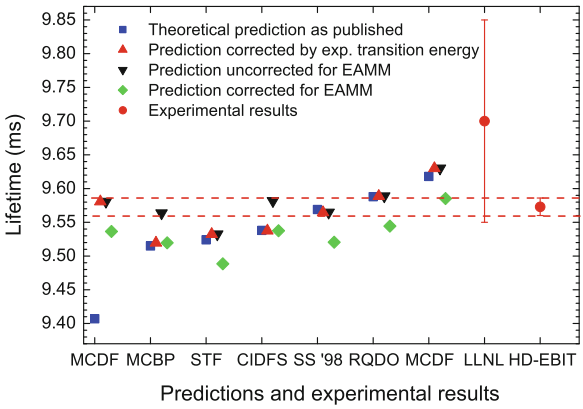

Fig. 10.13 A selection of predicted lifetimes of the $^2P_{3/2}$ first excited state in Ar^{13+} (see in corresponding order [175, 177–182]) and the experimental results of Ref. [31, 32] (*red dots* with error bars). *Dashed lines* uncertainty level. In all calculations, the electron anomalous magnetic moment (*EAMM*) contribution had been ignored, except in Refs. [175, 178]. See text for further details

Such isotope shifts are due to the isotopic change of the nuclear mass and the nuclear size, modifying the electronic wave function at short distances and thus shifting the binding energy. The mass shift, or recoil, contribution, is customarily separated into the normal and the specific mass shift terms. The relativistic recoil operator for a many-electron state is given by [89, 167, 184]

$$R_{ij} = \frac{\mathbf{p}_i \cdot \mathbf{p}_j}{2M} - \frac{Z\boldsymbol{\alpha}}{2Mr_i}\left(\boldsymbol{\alpha}_i + \frac{(\boldsymbol{\alpha}_i \cdot \mathbf{r}_i)\mathbf{r}_i}{r_i^2}\right) \cdot \mathbf{p}_j \,, \tag{10.16}$$

where relativistic units are used, and $\mathbf{r}_i$ and $\mathbf{p}_i$ are the position and the momentum, respectively, of a given electron indexed by i, and α_i stands for the Dirac matrices acting on the wave function of that electron. M denotes the nuclear mass and α is the fine-structure constant. The normal mass shift contribution is defined as the expectation value of $\sum_i R_{ii}$, and the specific mass shift term is given as the sum of the non-diagonal elements $\langle \sum_{i \neq j} R_{ij} \rangle$. Restricting Eq. (10.16) to the first term only yields the familiar non-relativistic mass shift operator. Atomic structure calculations of recoil effects based on the above operator are presented in Ref. [185]. A listing of the normal and specific mass shift terms NMS and SMS, together with the respective relativistic corrections RNMS and RSMS in Ar^{13+} is given in Table 10.2. These terms define the nuclear recoil effect up to the order $(\alpha Z)^4 m_e^2/M$, with m_e being the electron mass. The calculation of the QED contributions not included in the recoil operator is based on the article [90]. For an evaluation of these radiative terms, the use of QED beyond the Breit approximation is mandatory (see e. g., [184, 186]). The calculated shifts including relativistic recoil terms are in an excellent agreement with the experimental values. A calculation involving the non-relativistic recoil operator

Table 10.2 Numerical contributions of relativistic recoil and QED recoil terms to the total mass shift, and the field shift effect (^{36}Ar – ^{40}Ar) in the ground-state M1 transitions of Ar^{13+} and Ar^{14+} ions, in units of cm^{-1}. Results from [166]

Contribution	Ar^{13+}	Ar^{14+}
NMS	0.1052	0.0796
RNMS	−0.0822	−0.0627
One-electron QED	0.0002	0.0002
SMS	−0.0741	−0.0697
RSMS	0.1151	0.0887
Two-electron QED	−0.0008	−0.0015
FS	−0.0005	−0.0001
Sum	0.0629	0.0345

only would disagree with the experiment by a factor of approx. 2 (for Ar^{13+}) or 3 (for Ar^{14+}), as Table 10.2 shows.

10.6.5 The Hyperfine Structure of Hydrogenlike Ions

The most tightly bound electron, the $1s_{1/2}$, can give rise to an optical transition due to the hyperfine splitting (HFS) in heavy hydrogen-like ions in the presence of a nuclear spin. For heavy elements, the transition energy scales from the microwave region up to the visible spectrum, and even into the ultraviolet region in the case of bismuth. The magnetic hyperfine splitting of a hydrogenic ion with the electron being in a state described by the usual quantum numbers n, l and j may be generally represented in the form [187]

$$\Delta E_\mu = \frac{\alpha(Z\alpha)^3}{n^3} g_I \frac{m}{m_p} mc^2 \frac{F(F+1) - I(I+1) - j(j+1)}{2j(j+1)(2l+1)} \times \left[A_\mu(\alpha Z)(1-\delta)(1-\varepsilon) + x_{rad}\right] . \tag{10.17}$$

Here, Z is the atomic number, α is the fine-structure constant, m and m_p denote the mass of the electron and the proton, respectively, and c is the speed of light. I is the nuclear spin, F with $|I - j| \leq F \leq I + j$ is the total angular momentum quantum number of the ion, and $g_I = \mu/(\mu_N I)$ is the g factor of the nucleus, expressed in terms of the nuclear magnetic moment μ and the nuclear magneton μ_N. $A_\mu(\alpha Z)$ stands for the relativistic factor

$$A_\mu(\alpha Z) = \frac{n^3(2l+1)\kappa(2\kappa(\gamma + n_r) - N)}{N^4\gamma(4\gamma^2 - 1)}, \tag{10.18}$$

with the relativistic angular momentum quantum number $\kappa = 2(l-j)(j+1/2)$, and the further quantities $\gamma = \sqrt{\kappa^2 - (\alpha Z)^2}$, $N = \sqrt{n_r^2 + 2n_r\gamma + \kappa^2}$, $n_r = n - |\kappa|$. A_μ converges to unity in the non-relativistic limit. Equation (10.17) with keeping only the analytical relativistic factor $A_\mu(\alpha Z)$ in the square brackets describes the

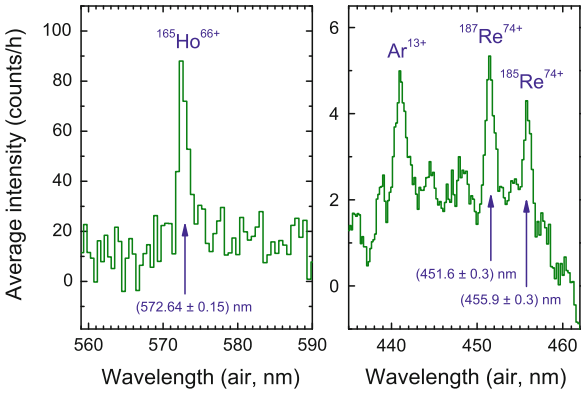

Fig. 10.14 Spectra from the hyperfine transition between the $F = 4 \rightarrow F = 3$ states in hydrogenlike Ho^{66+} (*left*) and $F = 3 \rightarrow F = 2$ states in hydrogenlike $^{185,187}Re^{74+}$ (*right*) [29, 189]

hyperfine splitting in the point-like nucleus approximation. Further corrections are introduced by the other parameters in the square brackets: δ is the nuclear charge distribution correction, ε is the nuclear magnetization (Bohr-Weisskopf) correction, and x_{rad} stands for the radiative correction, represented by self-energy and vacuum polarization diagrams. Further corrections arise due to the finite mass of the nucleus. The parameters δ and ε can be calculated assuming some nuclear model for the charge and magnetization distribution of the nucleus [187].

The first observation of HFS in HCI was achieved using the ESR storage ring at GSI [188]. Accelerated $^{209}Bi^{82+}$ ions produced by stripping were stored in the ring and excited by a laser which was tuned across the expected range. A fluorescence signal was obtained when the Doppler-shifted photon energy hit the $F = 4 \rightarrow F = 5$ transition between the ground state hyperfine levels. Shortly after, experiments at Super EBIT measured the corresponding transitions in Ho^{66+} (see Fig. 10.14), $^{173,175}Re^{74+}$, and $^{183,185}Tl^{80+}$ ions [189–191]. Later, the $^{207}Pb^{81+}$ ion was investigated, again at GSI [192]. Resonant laser excitation of the ground-state hyperfine transition in lithium-like bismuth performed at the storage ring ESR has been reported very recently [193]. Further studies will be required to reduce the uncertainties resulting from the Doppler shift.

Initially, the goal of the experiments had been to test QED contributions by means of the HFS of the hydrogenic systems: in contrary to measuring transition energies, which are mainly determined by the properties of the bound electron wave function at atomic distances (typically, a_0/Z, with a_0 being the Bohr radius), the value of the hyperfine splitting is dominantly determined by the behaviour of the electron wave function in the vicinity of the nucleus. Since the nuclear Coulomb field is strongest in this regime, measurements of the HFS can provide tests of QED in electric fields much stronger than those typical for binding energies. Experimental

errors in hyperfine splitting energies are also well below the magnitude of QED corrections.

However, very soon it turned out that uncertainties in the nuclear magnetization distribution, due to nuclear structural effects, were already sufficient to compromise the QED tests, since knowledge about the so-called hyperfine anomaly was not sufficiently accurate [194, 195]. The Bohr-Weisskopf effect resulting from this magnetization distribution was larger than the total QED correction, thus an investigation of QED terms by directly comparing experimental and theoretical hyperfine splitting is not possible. Additional problems might arise from the fact that nuclear magnetic moments were usually determined under conditions in which the diamagnetic correction, the shielding of external magnetic fields by the electronic shell, played a large role. While this correction plays less of a role in cases where atomic beam measurements are the source of the nuclear magnetic moment data than in the cases where nuclear magnetic resonance measurement with condensed probes were used, the calculation of this large correction factor also affects the final result. For these reasons, the measured wavelengths were used to determine the nuclear magnetization radii under different assumptions for the model magnetization distribution. In this way it became possible to quantify this elusive parameter, which otherwise can only be studied using muonic atoms. As an example, in the case of thallium the RMS value for the nuclear magnetic radius was determined with a fivefold increase in accuracy in comparison with previous work, to be 5.83 ± 0.14 fm and 5.89 ± 0.14 fm for the ^{203}Tl and ^{203}Tl isotopes, respectively [29].

As shown by Shabaev [196], the unwanted effect of not sufficiently well understood nuclear structural properties can be circumvented by employing a specific combination of hyperfine splitting values in hydrogen-like and lithium-like ions. In the following difference of the hyperfine splitting values of the different charge states,

$$\Delta' E = \Delta E^{(2s)} - \xi \Delta E^{(1s)}, \tag{10.19}$$

the parameter ξ can be chosen such that the Bohr-Weisskopf correction is largely cancelled. ξ can be calculated with sufficient accuracy, as it depends dominantly on the bound electron wave function and hardly on nuclear properties. For example, for bismuth ($Z = 83$), with $\xi = 0.16885$, a test of strong-field quantum electrodynamics on the percent level can be reached via $\Delta' E$, provided that the HFS values in both charge states can be measured with a relative accuracy of approx. 10^{-6} [196]. A similar procedure may be applied using boron-like and hydrogen-like ions of the same heavy element [197].

10.7 Resonant Photorecombination Processes

By choosing exactly the energy needed to excite dielectronic recombination resonances, far more selective excitation spectra can be obtained. Early EBIT measurements using this method were carried out by Beiersdorfer [198] on helium-like

Fe^{24+} and by Knapp et al. [199]. For the Fe ions, the energy resolution allowed to test dielectronic resonance strengths for individual resonances and compare them with predictions. Normalization was performed by comparison with the radiative recombination rate, which as a non-resonant process could be predicted theoretically with much smaller uncertainty.

10.7.1 Dielectronic Recombination

In the DR process, the cross section $\sigma^{\mathrm{DR}}_{i\to d\to f}(E)$ indicates the probability for electronic capture from an initial state i to a final state f under excitation of an intermediate, and often doubly-excited, state d:

$$\sigma^{\mathrm{DR}}_{i\to d\to f}(E) = \frac{2\pi^2\hbar^4}{p^2}\frac{A_r^{d\to f}}{\Gamma_d} L_d(E) V_{\mathrm{DC}}^{i\to d}\,. \tag{10.20}$$

Here, $p = \sqrt{(E/c)^2 - m^2c^2}$ represents the momentum of the projectile electron with a kinetic energy E. The energy dependence is conveniently represented with a Lorentzian profile

$$L_d(E) = \frac{\Gamma_d/(2\pi)}{(E_i + E - E_d)^2 + \frac{\Gamma_d^2}{4}}\,. \tag{10.21}$$

In this equation, Γ_d is the natural width of the intermediate state resulting from both radiative and auto-ionization decay channels: $\Gamma_d = \hbar A_r^d + \hbar A_a^d$. As mentioned above, the dielectronic capture rate V_{DC} and the Auger process rate are connected by the principle of detailed balance:

$$V_{\mathrm{DC}}^{i\to d} = \frac{2J_d + 1}{2(2J_i + 1)} A_a^{d\to i}\,. \tag{10.22}$$

The different density of initial and final states is accounted for with the multiplicities which follow from the total angular momenta of the intermediate J_d and the initial ionic state J_i, and the spin degeneracy of the initial continuum electron. Knowing that the Lorentzian function (10.21) is normalized to unity on the energy scale, i.e. $\int dE L_d(E) = 1$, and assuming for the electron momentum its resonance value $p_{res} = \sqrt{(E_d - E_i)^2/c^2 - m^2c^2}$, the strength of a DR resonance, i.e. the integrated area of a peak can be written as

$$S^{\mathrm{DR}}_{i\to d\to f} = \frac{2\pi^2\hbar^4}{p_{res}^2}\frac{2J_d + 1}{2(2J_i + 1)}\frac{A_r^{d\to f} A_a^{d\to i}}{\Gamma_d}\,. \tag{10.23}$$

If the final states are not resolved in an experiment, a summation over all possible such states, i.e. radiative decay pathways of the auto-ionizing states, has to be performed.

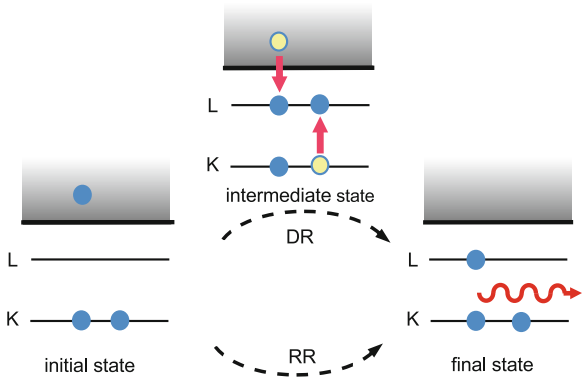

Fig. 10.15 Schematic representation of dielectronic (*top*) and radiative recombination (*bottom*), exemplified for KLL transitions in helium-like ions. The initial state of the total system consists of the ground-state ion and a continuum electron. After dielectronic capture, the ion is in an auto-ionizing intermediate state, which then relaxes by photon emission to a final state (which is not necessarily a ground state). The figure also illustrates that the initial and final states of RR and DR are indistinguishable, thus an interference of the two quantum pathways may occur

Also, usually in an EBIT experiment, it is not the above total cross section which is measured, but the photon intensity at a given angle with respect to the direction of the incoming electron beam. Therefore, the above formulas have to be corrected for the angular distribution of the X-ray emission [200–205] (Fig. 10.15).

Equation (10.23) allows one to derive a simple scaling law for the DR resonance strength with respect to the atomic number Z. As electron kinetic energies are much lower than the rest energy mc^2, the non-relativistic approximation may be used for the electron momentum, thus $1/p^2 \propto 1/E \propto 1/Z^2$. As noted before, for E1 transitions radiative rates are approximately proportional to Z^4, and the Auger rates are independent on Z, i.e. $A_a \propto V_{\mathrm{DC}} \propto Z^0$. Combining these, a non-relativistic scaling law of the following form can be derived for the DR resonance strength:

$$S^{\mathrm{DR}}_{i\to d\to f} \propto \frac{1}{aZ^2 + bZ^{-2}}\,, \tag{10.24}$$

with a and b being parameters depending on the actual rates and transition energy of the recombination channel. This function increases for low Z values, peaks usually in the intermediate Z region, and then decreases as $\propto Z^{-2}$.

The notion of dielectronic recombination (DR) was introduced by Massey and Bates in 1942 [206]. In 1964, Burgress used this process for the explanation of the temperature distribution of the solar corona. For a detailed historical treatment of DR until 1976, see the review article of Seaton and Storey [207].

The helium-like ions trapped in the LLNL EBIT were investigated with an electron beam of variable energy and an event-by-event data collection of the emitted X-rays and their energy as a function of the electron acceleration voltage [199, 208].

These experiments were reproduced and extended to other species in different laboratories. Investigations at the Berlin EBIT addressed channel-specific paths of dielectronic recombination in krypton ions including the heliumlike resonances [209].

Dielectronic resonances of helium-like Fe^{24+} [210], Xe^{52+} [37], I^{53+} [211] and heliumlike Ti^{20+}[212] were investigated by the Tokyo group, together with other isoelectronic sequences involving recombination into the $n = 2$ shell. The resonance strengths in the DR process with Ar^{16+} ions were measured by Smith et al. [213] at LLNL. He also studied the high n satellites of the Kα transition [214]. Tarbutt measured the dielectronic satellite transitions of the same ion under resonant excitation conditions [107], and Biedermann carried out similar measurements with the goal of improving plasma diagnostics in fusion research [136]. Relaxation of the doubly-excited intermediate state $1s^1\,2s^2\,J = 1/2$ through a two-electron one-photon transition in the KLL resonance array of Ar^{16+} were studied by Zou [215]. Zhang performed an investigation on Ge^{32+} [216].

Paralleling the experimental developments, extensive non-relativistic theories for the description of DR have been developed in the late 1970s and early 1980s, with the distorted wave formalism of Hahn et al. being an example [217, 218] (see also the review [207]). An extension to the relativistic case was carried out in several works, e.g. by Zimmerer et al. [219–221], by Chen and Scofield [37, 200], Pindzola [222]. The theoretical formalisms of Shabaev [84, 187] and Labzowsky et al. [223, 224] are based on relativistic field theory and allow a systematic treatment of radiative corrections and quantum interference effects.

10.7.2 Higher-Order Interactions in Photorecombination: Trielectronic and Quadruelectronic Terms

For the KLL resonances, the dielectronic recombination process had been generally understood to be the strongest photo-recombination channel. Beyond DR, however, higher-order processes may occur, in which the recombining electron simultaneously excites two or more bound electrons. These channels may be termed as trielectronic and quadruelectronic recombination (TR and QR, respectively), as three or four electrons are actively participating in the transition. These processes may be presumed to be weaker, since additional electron–electron interactions are needed to populate the intermediate states which are more highly excited than in the case of DR. However, experiments by Beilmann [225] showed that for some isoelectronic sequences, those processes were actually rather strong and in some cases dominant (see Fig. 10.16). The carbon-like ions in the range of atomic number $12 < Z < 26$ show trielectronic resonances as strong or stronger than the dielectronic ones.

For higher-order recombination processes, also the scaling of the resonance strength with Z is modified. In contrast to the dielectronic capture rates (10.22) which are largely independent on Z in the non-relativistic regime, trielectronic capture rates scale roughly as $1/Z^2$, since the additional Coulomb interaction among the

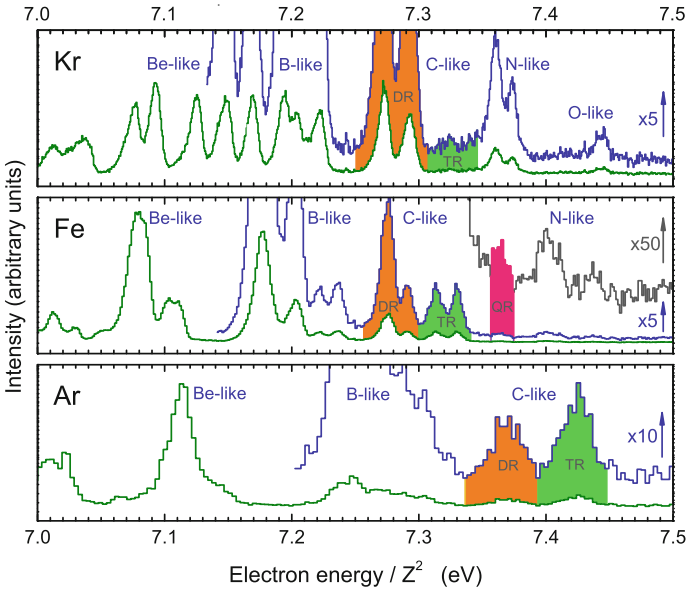

Fig. 10.16 Comparison of the X-ray fluorescence spectra following resonance recombination with carbon-like Ar, Fe, and Kr ions ($Z = 18, 26$, and 36). Trielectronic recombination (*TR*), barely resolvable in the case of Kr, gathers a larger total resonance strength than the dielectronic channel (*DR*) in the case of Ar (and other lighter elements). DR, TR and partially QR lines are marked by *orange*, *green* and *red* colours, respectively. The electron energies are normalized by Z^2 for a better comparison

electrons introduces a perturbative factor of $1/Z$ to the transition amplitude of the recombination step [225]. Thus, the scaling of the TR strength can be given as

$$S^{\mathrm{TR}} \propto \frac{1}{aZ^{-2} + b + cZ^4} \,. \tag{10.25}$$

This behavior has been confirmed experimentally by measuring the ratio of certain TR and DR strengths along the carbon-like isoelectronic series at different Z values ($Z = 18, 26, 36$) [225].

Theoretical models have to include the more complex intermediate states populated by the higher-order processes, and configuration mixing between the resonances corresponding to DR, TR, and QR in order not to neglect a fraction of the photo-recombination resonance strength. This has implications for the energy transfer within the radiative zone of stellar interiors, and for the ionization equilibrium of those and other astrophysical plasmas.

10.7.3 The Effect of the Breit Interaction in the Dielectronic Process

In atomic structure calculations and in the modelling of dynamical processes, the interaction between the electrons is usually approximated by the instantaneous Coulomb interaction. As known from the Bohr model, the normalized velocity v/c of atomic electrons can be approximated as $v/c = Z\alpha/n$, with n being the principal quantum number. This shows that in HCI with higher nuclear charge numbers, and, especially, in transitions involving inner-shell electrons, relativistic effects have to be taken into account. This does not only concern the bound-electron wave function, but also the inter-electronic interaction: as it is known even from classical considerations, the Lorentz force coupling a moving charged particle to the magnetic field induced by an other is proportional to v/c. Besides such current–current coupling effects, retardation also plays a role. A rigorous derivation of the electron–electron interaction can be made in the framework of QED. To the lowest order, the interaction of electrons is described by the one-photon exchange Feynman diagrams. In the Coulomb gauge, this yields to an effective interaction operator, which can be represented as the sum of the Coulomb and generalized Breit interactions:

$$V_{ij}(\omega) = V_{ij}^{C} + V_{ij}^{B}(\omega)\,, \tag{10.26}$$

with $V_{ij}^{C} = 1/r_{ij}$ and r_{ij} being the distance between two electrons. The generalized (or frequency-dependent) Breit interaction $V_{ij}^{B}(\omega)$ can be decomposed into the following parts:

$$V_{ij}^{B}(\omega) = V_{ij}^{\mathrm{magn}} + V_{ij}^{\mathrm{ret}} + V_{ij}^{\mathrm{ret}}(\omega)\,. \tag{10.27}$$

Here, the magnetic term is

$$V_{ij}^{\mathrm{magn}} = -\frac{\boldsymbol{\alpha}_i \cdot \boldsymbol{\alpha}_j}{r_{ij}}\,, \tag{10.28}$$

and the retardation of the scalar and the transverse interaction in the Breit approximation is described by the operator

$$V_{ij}^{\mathrm{ret}} = \frac{\boldsymbol{\alpha}_i \cdot \boldsymbol{\alpha}_j}{2r_{ij}} - \frac{(\boldsymbol{\alpha}_i \cdot \mathbf{r}_{ij})(\boldsymbol{\alpha}_j \cdot \mathbf{r}_{ij})}{2r_{ij}^3}\,. \tag{10.29}$$

The sum of V_{ij}^{magn} and V_{ij}^{ret} is the usual (frequency-independent) Breit interaction V_{ij}^{B}. Additional retardation effects are described by a term which depends explicitly on the frequency of the exchanged virtual photon: ω:

$$V_{ij}^{\mathrm{ret}}(\omega) = -\boldsymbol{\alpha}_i \cdot \boldsymbol{\alpha}_j \frac{\cos(\omega r_{ij}) - 1}{r_{ij}} + (\boldsymbol{\alpha}_i \cdot \boldsymbol{\nabla}_i)(\boldsymbol{\alpha}_j \cdot \boldsymbol{\nabla}_j) \frac{\cos(\omega r_{ij}) - 1 + \omega^2 r_{ij}^2/2}{\omega^2 r_{ij}} . \tag{10.30}$$

Here, $\boldsymbol{\nabla}_i$ denotes differentiation with respect to the position vector of the ith electron. It has been recognized soon that such effects largely influence the energy levels in heavy atoms and ions [226]. Cheng, Johnson et al. [123, 129, 227] found that even higher-order Breit interactions contribute at the level of 0.1 eV and that inclusion of frequency-dependent and other high-order many-body corrections was necessary in order to extract QED contributions from the accurate experimental data.

A strong influence of the Breit interaction to the dielectronic capture rates have been predicted by different groups [200, 219]. This effect was experimentally confirmed in EBIT measurements by Nakamura and his team [43] through comparison of the resonance strengths to calculations with and without the inclusion of the Breit interaction in the capture matrix elements. In a recent experiment, also at the Tokyo-EBIT [228], a measurement of the intensity of an X-ray decay following dielectronic capture into lithium-like Au ions at 90° has confirmed the dominance of the Breit interaction in the angular distribution of certain transitions, predicted by Fritzsche et al. [205].

10.7.4 Quantum Interference Terms Between Dielectronic and Radiative Recombination

For very high charge states, the RR cross Eq. 10.11 become very large. Intuitively, this results from the strong nuclear field. At the same time, electron–electron correlations do not change much with the ionic charge, and, as also Eq. (10.24) shows, dielectronic resonances decrease and partly lose their dominating role in photo-recombination. Thus, the quantum mechanical transition amplitudes for the direct and resonant recombination channels may become comparable. Since the initial and final states of both channels may be the same, as shown in Fig. 10.15, quantum interference of the two processes can occur. This situation is analogous to the case of photo-ionization, for which a modification of the line shapes due to interference was described by Fano [229]. The total cross section of photo-recombination including interference effects is given by [221, 230–232]

$$\sigma^{\mathrm{PR}}_{i\to d\to f}(E) = S^{\mathrm{DR}}_{i\to d\to f} \frac{2}{\Gamma_d \pi} \frac{1 - 1/q^2 + 2\varepsilon/q}{1 + \varepsilon^2} , \tag{10.31}$$

with q being the Fano interference parameter [221, 229–231], and the unitless energy is $\varepsilon = 2(E + E_i - E_d)/\Gamma_d$. For large q values, the asymmetric Fano line shape converges to the symmetric Lorentzian one, i.e. $\lim_{q\to\infty} \sigma^{\mathrm{PR}} = \sigma^{\mathrm{DR}}$. Calculations for

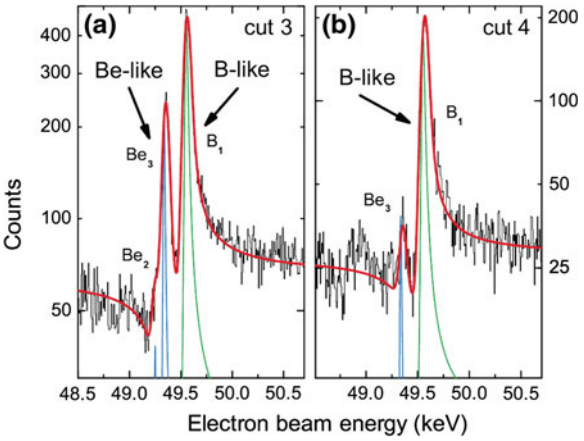

Fig. 10.17 Fano *line shapes* observed in the X-ray fluorescence spectra following KLL photo-recombination with beryllium- and boron-like Hg ions. The experimental data is shown in *black*, and a fit curve in *red* (Fano profile convoluted with a Gaussian function to account for experimental line broadening). Normalized non-convoluted theoretical cross sections are shown in *blue* and *green* for the beryllium- and boron-like charge state, respectively. Figure taken from Ref. [63]

the photo-recombination of highly charged heavy ions taking into account quantum interference effects between DR and RR have been performed by several groups [221–223, 233, 234].

Since the increase of the radiative widths renders the resonances also rather broad in the high-Z range, studies of resonance profiles by tuning the electron beam energy became possible. Observations were made for helium- to boronlike uranium ions in the Super-EBIT [235], and with highly charged mercury ions using the Heidelberg EBIT [63], as shown in Fig. 10.17. Further experimental observation of the interference effect has been performed with beryllium-like bismuth ions using the Tokyo-EBIT [236]. The q parameters of the Fano profiles was extracted and compared with theory in Ref. [237].

10.7.5 Resonant Photo-Ionization Processes

The first demonstration of photo-ionization of HCI using an EBIT quickly gave way to detailed studies in the soft X-ray region [45–47]. Much higher charge states were accessed than in earlier work using synchrotron radiation, where merged ion-photon beams were used to study resonant K-shell PI of C^{4+} at photon energies near 300 eV, and also charge states as high as 7+ in Xe. However, ionization potentials were limited to around 150 eV due to insufficient ion beam area densities. With the EBIT method, Fe^{14+} and Ar^{12+} were addressed, with four times higher ionization potentials and with high spectral resolution. The results for iron (see Fig. 10.18 showed remarkable

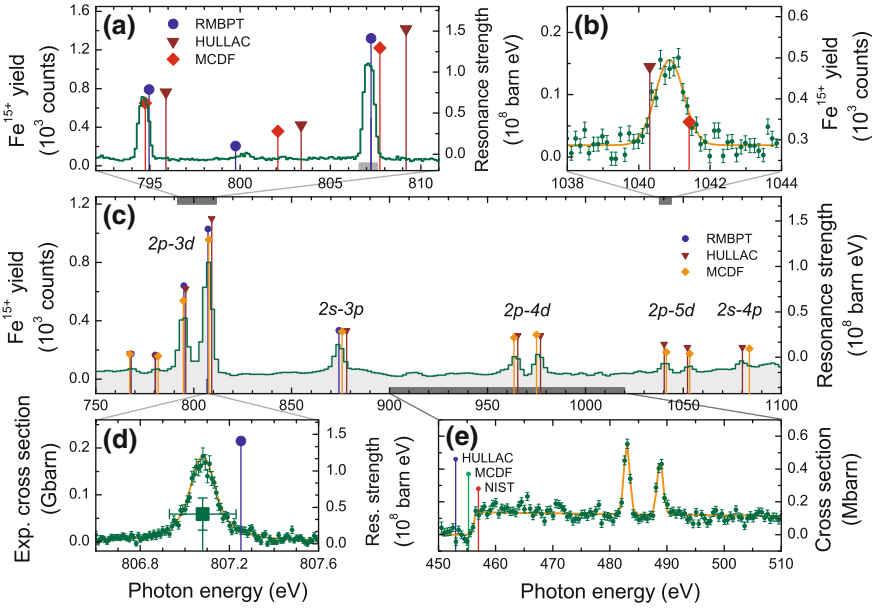

Fig. 10.18 Photoion yield after irradiation of Fe^{13+} with synchrotron radiation as a function of the photon energy [47]. Panel **c** overview scan; **a**, **b**, **d** detailed scans of various resonances; **e** ionization edge and second-order photon lines. Theoretical values: RMBPT: *blue circles* (Ref. [238]); HULLAC: *brown triangles*; MCDF: *orange circles* (both from Ref. [47])

disagreement with several predictions, but also a very consistent agreement with the relativistic many-body perturbation theory (RMBPT) calculations of Gu [238] at the level of meV.

Fano quantum interference of direct and resonant photoionization in the X-ray regime, analogously to interferences in recombination processes discussed above, has been observed with EBIT methods by Simon et al. [46].

10.8 Photonic Excitation: Laser Spectroscopy from the Visible to the X-ray Range

One of the great advantages of EBITs is the linear structure of the ensemble of trapped ions. The ion density can be estimated simply by assuming that the negative space charge of the electron beam of a density n_e (which can be as high as $n_e = 10^{13}$ cm^{-3}) is compensated in part by the positive ions of charge state q_{ion} it traps. Thus, a typical ion density is $n_{ion} < 0.3 \times n_e/q_{ion}$. If the interacting beam overlaps with the ion cloud axially, the ion target area density results from integrating over a trap length of a few centimeters, giving thus values of 10^{10} cm^{-2} ions. By comparison,

the density of the residual gas background at pressures down to 10^{-13} mbar found in a cryogenic EBIT can be as low as 3,000 neutrals/cm^3. Therefore, the photon beam interacts mainly with the ion target and very little with the residual gas.

10.8.1 Laser Spectroscopy in the Soft X-ray Region at Free-Electron Lasers

While laser spectroscopy had become by the end of the twentieth century an established method in atomic physics, and its applications to various fields of science had unleashed very rapid progress in the understanding of the electronic structure of atoms and molecules, metrology, remote sensing and many other branches, the vacuum ultraviolet region had only been touched by two-photon laser spectroscopy of the Lyman-α lines in the hydrogen atom. The cause for this status was primarily the lack of practical lasers in this spectral range. The few demonstrations of X-ray lasers based on collisional excitation within plasmas generated by pulsed optical lasers in the kilojoule range [240, 241] or table-top devices using electrical discharges [242] did not provide tunable beams, and required a very complex operation. The situation changed with the introduction of free-electron lasers (FEL) capable of generating the sought-after short wavelengths [243]. By changing the acceleration and undulator parameters, it was now possible to scan the photon energy across a wide range, and repetition rates on the order of 100 Hz were within reach. The Tesla Test Facility, later renamed FLASH (Free-Electron LASer in Hamburg) opened its doors as an experimental user facility in 2005 and enabled a large variety of novel experiments [244]. The Freiburg EBIT group had already started with the design of an experiment involving an EBIT as a target of HCI for FEL laser spectroscopic studies. The so-called Tesla (later FLASH) EBIT, a transportable device, came into operation in the year 2006 [39] and was installed at FLASH. There, the Fe^{23+} ions produced and stored within the device were exposed to the FLASH pulses (see Fig. 10.19), and the transition $2s_{1/2} \rightarrow 2p_{1/2}$ was resonantly excited by them at a photon energy of 48.6 eV. A coincidence detection method enormously reduced the background. Since the bandwidth of the radiation from FLASH was broad, an in-line grating monochromator had to be used to reduce it to an acceptable level [39, 239]. The experiment with Fe^{23+} achieved an excellent level of statistical accuracy, but calibration and stability of the in-line monochromator were not commensurate, and a systematic calibration error of 0.15 eV remained. However, due to the high ion production rate of that experiment, an accompanying measurement using a flat-field spectrometer could improve earlier results and brought the total uncertainty to a level of 4 ppm.

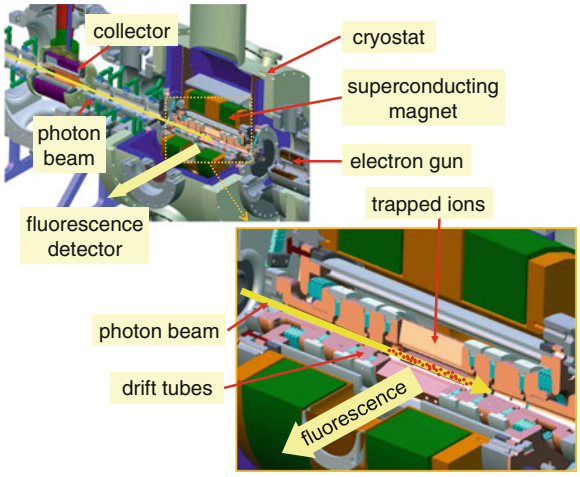

Fig. 10.19 X-ray laser spectroscopy setup with FLASH EBIT [39, 48, 239]. The monochromatic photon beam from a free-electron laser or synchrotron radiation source enters through the hollow collector and interacts with the trapped ions in the central drift tube region (zoomed insert). X-ray resonance fluorescence is detected through the viewports arranged around the cryostat

10.8.2 Extending Laser Spectroscopy into the X-ray Domain

The next step followed with the commissioning of the Linac Coherent Light Source (LCLS) at SLAC in Menlo Park, California. The FLASH EBIT was attached to the SXR monochromator beamline in order to analyze the strongest transitions in Fe^{16+}, an ion of utmost astrophysical importance. The question being addressed here was the existing discrepancy between advanced theory and astrophysical as well as plasma observations with regard to the intensity ratio of the strongest transitions in its spectrum [48, 49] (Figs. 10.20, 10.21).

Very recently, this method has been demonstrated for excitation of the strongest transitions in helium-like Fe^{24+} and in lithium-like Fe^{23+} by Rudolph and colleagues [140], and for Kr^{34+} by Steinbrügge et al. Fig. 10.22 shows an overview spectrum and individual line scans obtained with FLASH EBIT using a hard X-ray beamline equipped with a double undulator [245] at PETRA-III. The stability of the available monochromator permitted high resolution scans, yielding accurate energies (see Table 10.3 and also line widths (see plot on the bottom of Fig. 10.22). The measured energies confirm bound-state QED predictions by Artemyev et al. for the helium-like [131] and lithiumlike [141] charge states, and point out the need of extending such calculations to ions with more electrons. By using two detectors, one of them parallel to the polarization plane of the incoming radiation, and one perpendicular, the fluorescence emission characteristics of the different transitions can be recorded. Since for helium-like Fe^{24+}, the intercombination line y has a narrower natural line width than the resonance transition w, the line profiles are distinct and can

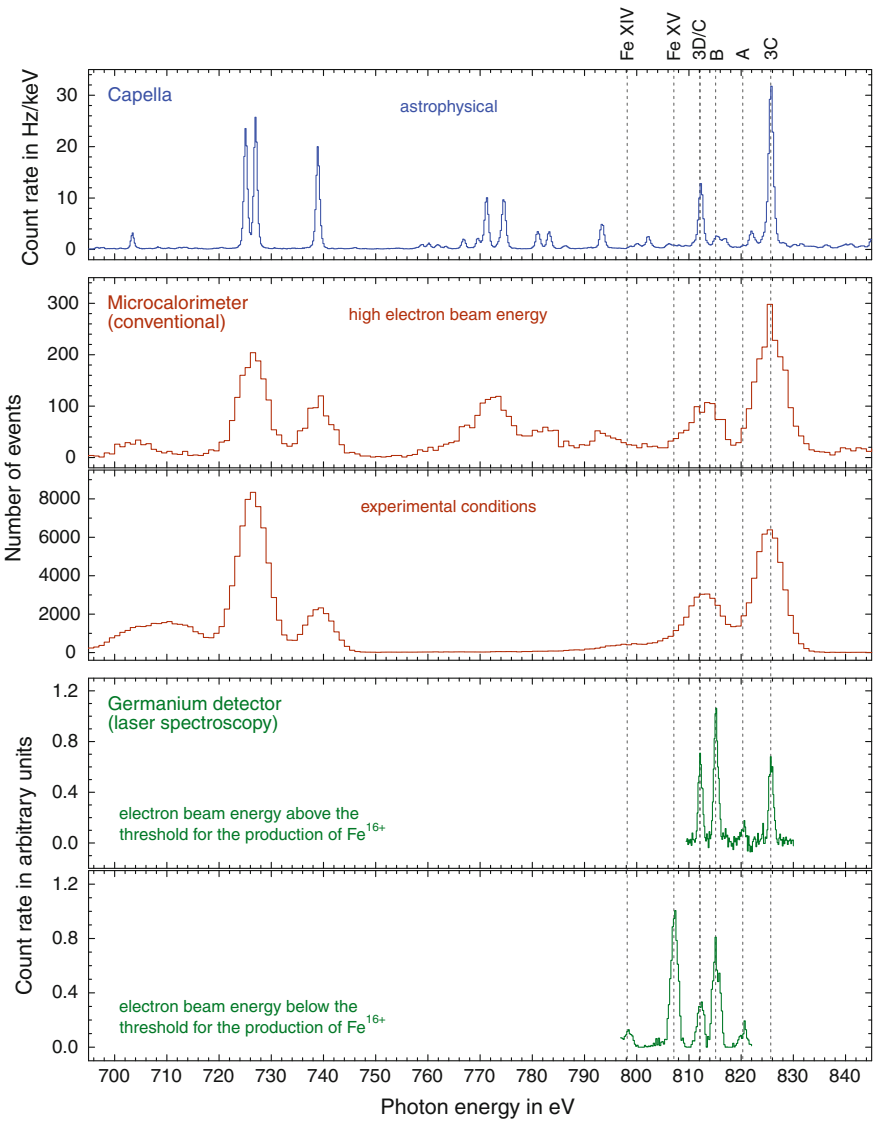

Fig. 10.20 Comparison of astrophysical emission spectra of highly charged iron ions (from Capella) with data from FLASH EBIT. *Blue* Grating spectrometer data from Capella. *Red* Microcalorimeter spectra obtained under different EBIT conditions. *Green* Soft X-ray laser spectroscopy results [48, 49] obtained at the LCLS free-electron laser facility

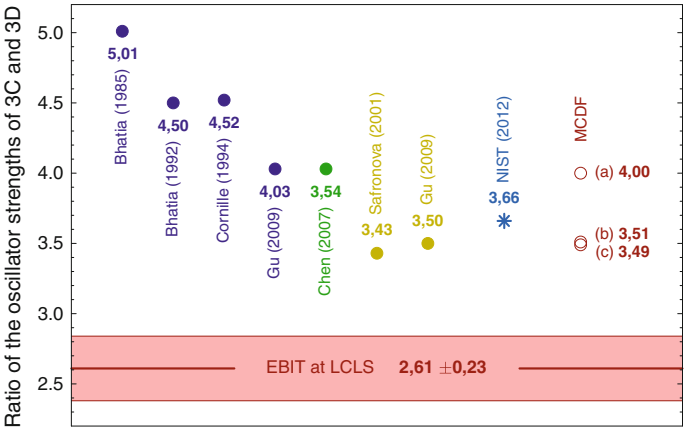

Fig. 10.21 Ratio 3C/3D of the oscillator strengths of the strongest soft X-ray transitions in neonlike Fe^{16+} obtained with various theoretical methods, in comparison with the X-ray laser spectroscopy result obtained at LCLS [48]. The significant and consistent discrepancy points to a probably insufficient inclusion of electron–electron correlation contributions in the theoretical approaches

be fitted with a Voigt profile, yielding a Gaussian component resulting from instrumental effects and ion temperature, and a Lorentzian width corresponding to the transition rate. The example shown indicates a trapped ion temperature of less than 30 eV, resulting from strong evaporative cooling. These initial results clearly that in the near future, combining synchrotron radiation filtered by high-resolution monochromators with trapped HCI will help overcoming current limitations of emission spectroscopy, which has always to compromise spectral resolution for signal strength.

10.8.3 Laser Excitation of Forbidden Transitions in the Visible Range

Many years there has been a strong interest in laser spectroscopic studies with highly charged ions. Preparations for an experiment using beryllium-like Ar^{14+} were carried out already at the Oxford EBIT [248]. The RETRAP program at LLNL [249] had the aim of sympathetically cooling HCI for their use in laser spectroscopic studies. Laser spectroscopy on trapped HCI was first achieved in Heidelberg by Mäckel et al. [250] using Ar^{13+} ions. Here, a pulsed tunable laser was used in a collinear geometry for excitation of the E1-forbidden transition $2p^2P_{3/2} \rightarrow 2p^2P_{1/2}$ within the ground-state configuration of the ion. Due to its M1 character with a long decay time of 9.7 ms [31], detection of fluorescence radiation had to rely on the magnetic-trapping mode operation of the EBIT. The setup is sketched in Fig. 10.23. For the measurement the following cyclic scheme was applied: After ion production, the electron beam is turned off, and after a suitable decay time for the electron-impact excited ions, the

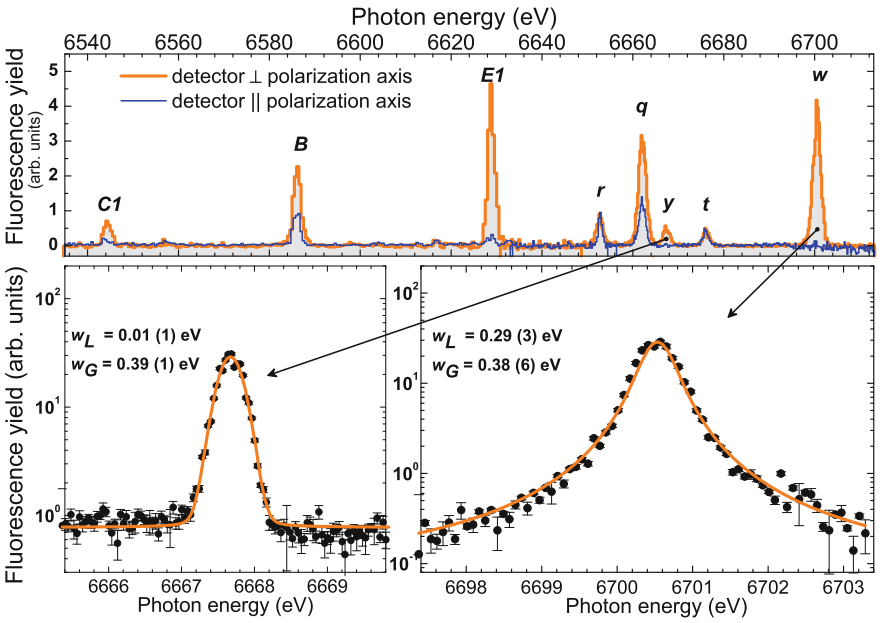

Fig. 10.22 *Top* Overview fluorescence spectrum of helium-like, lithium-like and beryllium-like Fe ions using two detectors aligned differently to the polarization plane of the incoming photon beam: (*red*) perpendicular to polarization axis, and (*blue*) parallel to polarization axis. *Bottom left* Scan over the intercombination line (*y*) $1s^2\,{}^1S_0 \rightarrow 1s\,2p\,{}^3P_1$. *Bottom right* Scan over the resonance transition (*w*) $1s^2\,{}^1S_0 \rightarrow 1s\,2p\,{}^1P_1$. The fitted Gaussian and the Lorentzian widths w_G and w_L of the transitions are shown [140]

fluorescence intensity after the laser excitation pulses is recorded as a function of their wavelength. Simultaneously, evaporative cooling [12] was applied in order to reduce the thermal width of the lines, which is very high due to the deep ion trapping potential in the EBIT. In this way, the translational ion temperature was lowered from values above 10^6 K down to the range of 10^5 K. Figure 10.24 shows the time evolution of the fluorescence signal and the ion temperature during the wavelength scans. One can observe how the width of four Zeeman components becomes smaller during the cooling cycle. The resulting wavelength of 441.25568(26) nm agrees excellently with earlier measurements carried out with grating spectrometers (441.2559(1) nm [165], and 441.2556(1) nm [168]). The currently most elaborate theoretical prediction of 441.261(70) nm [176] has a much larger uncertainty. Higher resolution would be possible if the trapped ions could be cooled even more. However, temperatures low enough (in the mK and lower range) for very high resolution laser spectroscopy are extremely difficult to achieve in this EBIT environment. A direct application of laser cooling schemes is currently not possible due to the long lifetimes of the forbidden transitions, and also to the lack of allowed transitions in the optical range. Most likely, future experiments will have to rely on the use of sympathetic cooling using external ion traps coupled to an EBIT.

Table 10.3 X-ray transitions of helium-like, lithium-like, beryllium-like, boron-like and carbon-like transitions resonantly excited from the ground state with synchrotron radiation. X-ray fluorescence was detected as a function of photon energy. Energies are given in units of eV; the calibration is based on the absorption edge technique [140]

	Transition	Experiment	Theory	Reference
w	$1s^2\,{}^1S_0 \rightarrow 1s\,2p\,{}^1P_1$	6700.549(5)(70)	6700.4347(11)	[131]
			6700.490	[118]
y	$1s^2\,{}^1S_0 \rightarrow 1s\,2p\,{}^3P_1$	6667.671(3)(69)	6667.5786(12)	[131]
			6667.629	[118]
t	$1s^2\,2s\,{}^2S_{1/2} \rightarrow 1s\,2s\,2p\,{}^2P_{1/2}$	6676.202(3)(69)	6676.129(47)	[141]
			6675.87	[246]
q	$1s^2\,2s\,{}^2S_{1/2} \rightarrow 1s\,2s\,2p\,{}^2P_{3/2}$	6662.240(6)(69)	6662.188(11)	[141]
			6661.88	[246]
r	$1s^2\,2s\,{}^2S_{1/2} \rightarrow 1s\,2s\,2p\,{}^2P_{1/2}$	6652.826(3)(69)	6652.776(25)	[141]
			6652.58	[246]
E	$1s^2\,2s^2\,{}^1S_0 \rightarrow 1s\,2s^2\,2p\,{}^1P_1$	6628.804(5)(68)	6631.057	[247]
B	$1s^2\,2s^2\,2p\,{}^2P_{1/2} \rightarrow 1s\,2s^2\,2p^2\,{}^2P_{1/2},\ {}^2D_{3/2}$	6586.085(7)(67)	6586.7	[140]
C	$1s^2\,2s^2\,2p^2\,{}^3P_0 \rightarrow 1s\,2s^2\,2p^3\,{}^3D_1$	6544.225(4)(66)	6544.8	[140]

A similar scheme was recently applied by Schnorr et al. [251] to the study of the so-called Fe XIV*green coronal line*, yielding a result of 530.2801(4) nm. This astrophysically essential line was discovered in the solar corona during the solar eclipse of 1869 [252], and originally even a new element, *coronium*, was postulated as its source. Eventually, it was explained in the 1940s by Grotrian [253] and Edlén [254] as arising from the Fe^{13+} ion, thus giving the first hint on the high temperature of the solar corona. However, in spite of its widespread use in astrophysical plasma diagnostics, no laboratory measurement of its wavelength had hitherto been reported.

10.9 Ion Cooling Schemes for Spectroscopy with HCI

In recent years, singly charged trapped ions have shown their ideal suitability as excellent frequency standards [255, 257–260], in particular if combined with frequency combs [261–263]. Sympathetic cooling (see e.g., [264] allows for preparing extremely cold samples of ions for this purpose. Among the number of open scientific questions which are aimed at, the constancy of Nature's laws stands out. A possible time variation of fundamental constants, and very prominently of the fine-structure constant α appears in various theories [265]. HCI offer new possibilities [266] due to their intrinsic, advantageously low polarizability and strong α binding energy dependence.Several schemes that make use of particular isoelectronic sequences have been proposed [266–273].

A central problem for laser spectroscopy with EBITs arises from the high translational temperature of the trapped ion ensemble, which is the result of the ionization by

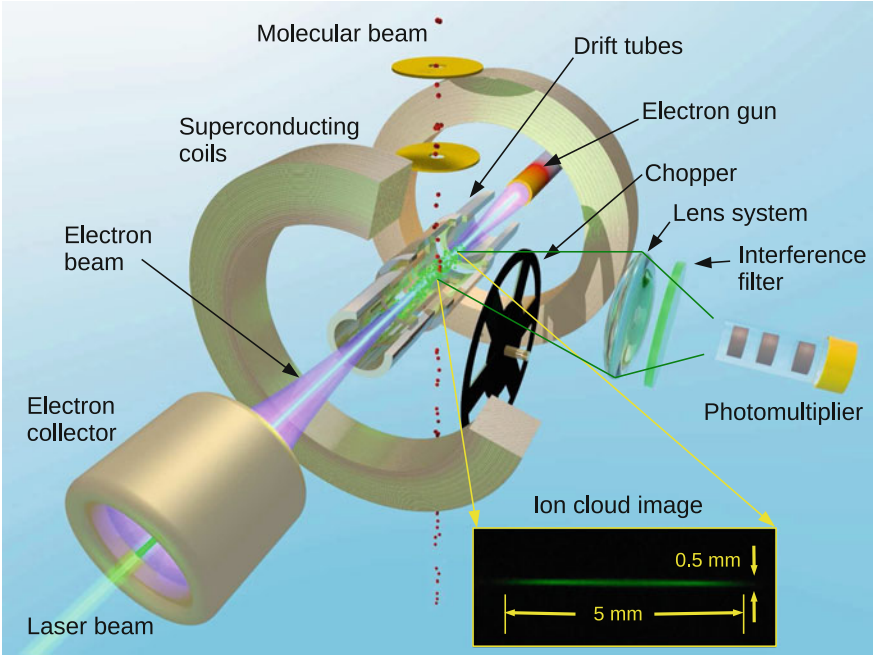

Fig. 10.23 Experimental setup for laser spectroscopy [251] of the forbidden transition $1s^2 2s^2 2p^2 P_{3/2} \rightarrow^2 P_{1/2}$ in Ar^{13+}. *Side* photograph of the ion cloud. A pulsed tunable laser irradiates the trapped ions along the trap axis. Their fluorescence upon resonant excitation of forbidden transitions decays slowly with a lifetime of several ms, and is collected by a hollow light guide and detected with a photomultiplier. A chopper and an interference filter are used to reduce the background during and after the pulses

electron impact. Evaporative cooling [250] does not solve this problem, even though the the ion temperature is largely reduced. Since the cooling starts at $T > 10^6$ K, the decrease to $T < 10^5$ K does not represent a substantial advantage for metrology purposes. Here, a different approach has to be implemented. The RETRAP experiment [249] implemented resistive ion cooling and later succeeded in sympathetically cooling HCI within a laser-cooled crystal of Be^+ ions [274] in a Penning trap. However, that method does not provide the advantages of Paul traps, which offer a field-free region at the trap center and no shifts due to the Zeeman effect. For this purpose, the Heidelberg group has initiated a program using a novel cryogenic linear Paul trap, CryPTEx [275] built for that purpose [276]. Both the storage of HCI over time scales amenable for laser spectroscopy, and reduction of interactions with blackbody radiation set very exacting requirements for this experiments (see Fig. 10.25). Quantum-logic methods [278] and similar schemes based on interrogating the coherent motional states of co-trapped ions ([279]) would offer a tool for detection of extremely long-lived states [280] in the optical domain. Furthermore, applications to the X-ray region have been proposed [281].

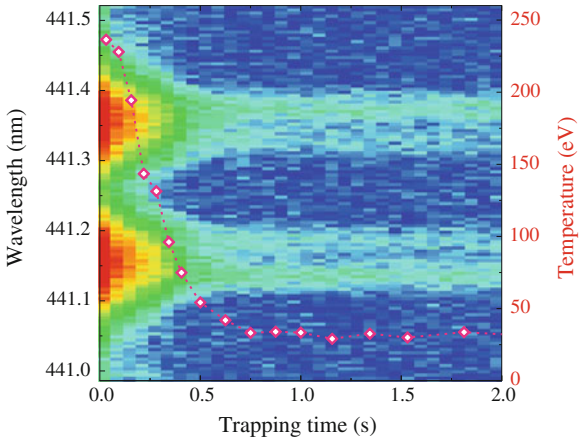

Fig. 10.24 Intensity of the resonant fluorescence of the forbidden M1 transition $1s^2 2s^2 2p^2 P_{3/2} \rightarrow^2 P_{1/2}$ in Ar^{13+} while scanning the laser wavelength (*vertical axis*) versus trapping time under conditions of evaporative cooling [250]. The Zeeman π components are observed in perpendicular direction to the magnetic field axis. Their linewidth decreases with increasing trapping time as the ion temperature (*right scale*) is reduced by evaporative cooling. At the same time, the related ion losses degrade the signal-to-noise ratio

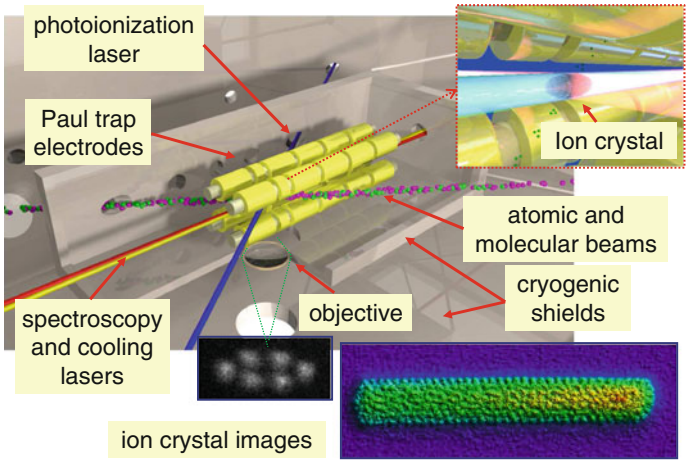

Fig. 10.25 Principle of operation of the cryogenic linear Paul trap CryPTEx [275]. Be^+ ions are produced by photo-ionization of Be atoms from an atomic beam. Laser-cooled ion crystals of Be^+ (images show a Mg^+ and a mixed $Mg^+ + MgH^+$ ion crystal) are used to sympathetically cool highly charged ions produced in an EBIT. The 4 K cryogenic environment enables a vacuum on the order of 10^{-14} mbar and decouples the trapped ions from thermal radiation causing undesired shifts in the laser transitions of interest. One long term goal of this experiment is studying the possible time variation of the fine-structure constant α using quantum-logic readout of forbidden transitions in the trapped highly charged ions [277]. Predictions indicate that the frequencies of some of those transitions have an extremely high sensitivity to the value of α [266]

10.10 Summary and Future Directions

Nearly three decades of spectroscopy with EBITs have boosted our knowledge of QED and relativistic effects in the electronic structure of the ubiquitous HCI. New directions have surged with the advent of free-electron lasers and extremely intense X-ray sources. An interesting new field which has not yet been exploited for HCI research is the use of laser-generated high harmonics in the femtosecond and attosecond range. These compact sources of VUV radiation will soon become a workhorse of atomic physics, and their combination with trapped HCI seems a logical consequence. Cold crystals offer interesting possibilities not only in the visible and UV regions, but also for the detection of X-ray photons, since the heating of the crystal by the recoil due to photon emission and absorption in the X-ray domain becomes appreciable [282]. In combination with synchrotron radiation sources and X-ray free-electron lasers, this might prove to be a very powerful technique for X-ray spectroscopy with sympathetically cooled ions.

Nuclear excitation effects resulting from interactions with the electronic shell are an important and nearly unexplored field [283]. High resolution laser spectroscopy of fine and hyperfine structure will achieve a far higher sensitivity to those effects as the overlap of electronic wave functions with the nucleus is strongly enhanced in HCI. An interesting alternative approach are proposed investigations of circular states in Rydberg states of HCI [284], in which nuclear size effects can be made weaker in order to address other physical parameters of e.g., QED with lower uncertainties.

X-ray metrology is currently bound to the use of crystals as standards of length. However, their suitability beyond the parts-per-billion accuracy is seriously compromised by various solid state effects. The most serious problem is thermal expansion, implying that a temperature stability on the order of mK is needed for achieving such an accuracy. In contrast, electronic transitions in HCI are per se insensitive to external effects to a much higher degree. Even the allowed X-ray transitions in HCI, in spite of their rather large natural width, provide truly stable standards in this region. Forbidden transitions of different types would allow for an stability far beyond any other standards currently in sight, including Mössbauer transitions in nuclei, since they are sensitive to the strong fields within their host crystals. Trapped HCI can provide a very large number of transitions to be used as standards at much higher frequencies (10^{20} Hz) than the current optical clocks (10^{16} Hz). The possible applications that such fast-running clocks would afford for both technology and fundamental scientific studies can only be dreamed of.

Acknowledgments The authors are indebted to a large number of colleagues which whom they had the opportunity and pleasure to collaborate with over the years. Explicitly, I (JRCLU) would like to thank to Peter Beiersdorfer, who has been a steady source of ideas for me and for this field in general. I also would like to thank to other EBIT colleagues at LLNL, like Greg V. Brown and Klaus Widmann, who worked closely with him and me. In both Freiburg and Heidelberg, EBIT science was always strongly backed by Joachim Ullrich and also by my colleages Robert Moshammer, Alexander Dorn and Claus-Dieter Schröter. Ideas, contributions and constant work of former and current EBIT students and postdocs have been the basis of the experiments in Freiburg and Heidelberg: Here I would like to mention Bhas Bapat, Andreas Werdich, Ilija Draganič, Christina Dimopolou, Panlin

Guo, Xuemei Zhang, Alexandra Rohr, Antonio González Martínez, Rosario Soria Orts, Johannes Braun, Hjalmar Bruhns, Vladimir Mironov, Sascha Epp, Günther Sikler, Alain Lapierre, Günter Brenner, Volkhard Mäckel,Katharina Kubiček, Lodeweijk Arntzen, Martin Simon, Guiyun Liang, Renee Klawitter, Rainer Ginzel, Benjamin Schmitt, Maria Schwarz, Thomas Baumann, Kirsten Schnorr, Franziska Brunner, Stuart Higgins, Christian Beilmann, Sven Bernitt, Oscar Versolato, Sebastian Georgi, Jan Rudolph, René Steinbrügge, Alexander Windberger, James Harries, and Hendrik Bekker. Profs. Yaming Zou, Hiroyuki Tawara and Paul Mokler have been our long-time guests, and both their help and stimulating discussions are greatly appreciated. I would also like to mention my collaborations in this field with the groups of Klaus Blaum at MPIK, Jens Dilling at TRIUMF, Fritz Aumayr at TU Vienna, Michael Drewsen in Aarhus, and Piet Schmidt at PTB. Crucially, a strong theory support by the division led by Christoph Keitel was essential for these works. Last but not least, nothing could have been achieved without the craftsmanship of the technicians of our mechanical workshops and work group. Of those companions, Karl Bechberger, Norbert Müller and Christian Kaiser deserve our particular gratitude for their year-long commitment. ZH would like to thank in addition for fruitful collaboration and insightful conversations with Natalia Oreshkina, Jacek Zatorski, Adriana Pálffy, Roxana Schiopu, Stefano Cavaletto, Octavian Postavaru, Ioannis Stasinopoulos, Matthias Gail, Stephan Balliel-Zakowicz, Anton Artemyev, Ilya Tupitsyn, Vladimir Yerokhin, Vladimir Shabaev, Ulrich Jentschura, Werner Scheid and Christoph Keitel.

References

1. J. Sapirstein, K.T. Cheng, Tests of quantum electrodynamics with EBIT. Can. J. Phys. **86**, 25 (2008)
2. R.E. Marrs, S.R. Elliott, D.A. Knapp, Production and trapping of hydrogenlike and bare uranium ions in an electron beam ion trap. Phys. Rev. Lett. **72**, 4082 (1994)
3. R.E. Marrs, P. Beiersdorfer, D. Schneider, The electron-beam ion trap. Phys. Today **47**, 27 (1994)
4. B.M. Penetrante, J.N. Bardsley, D. Dewitt, M. Clark, D. Schneider, Evolution of ion-charge-state distributions in an electron-beam ion trap. Phys. Rev. A: At. Mol. Opt. Phys. **43**, 4861 (1991)
5. E.D. Donets, The electron beam method of production of highly charged ions and its applications. Phys. Scr. T **3**, 11 (1983)
6. E.D. Donets, Electron beam ion sources and associated physics at JINR. Nucl. Instrum. Methods Phys. Res. Sect. B **9**(4), 522 (1985)
7. J. Arianer, C. Collart, C. Goldstein, H. Laurent, M. Malard, Status report of the Orsay EBIS program. Phys. Scr. T **3**, 35 (1983)
8. M.A. Levine, R.E. Marrs, J.R. Henderson, D.A. Knapp, M.B. Schneider, The electron beam ion trap: A new instrument for atomic physics measurements. Phys. Scr. **22**, 157 (1988)
9. M.A. Levine, R.E. Marrs, J.N. Bardsley, P. Beiersdorfer, C.L. Bennett, M.H. Chen, T. Cowan, D. Dietrich, J.R. Henderson, D.A. Knapp, A. Osterheld, B.M. Penetrante, M.B. Schneider, J.H. Scofield, The use of an electron beam ion trap in the study of highly charged ions. Nucl. Instrum. Methods Phys. Res. Sect. B **43**, 431 (1989)
10. D. Schneider, M.W. Clark, B.M. Penetrante, J. McDonald, D. Dewitt, J.N. Bardsley, Production of high-charge-state thorium and uranium ions in an electron-beam ion trap. Phys. Rev. A: At. Mol. Opt. Phys. **44**, 3119 (1991)
11. D.A. Knapp, R.E. Marrs, S.R. Elliott, E.W. Magee, R. Zasadzinski, A high-energy electron beam ion trap for production of high-charge high-Z ions. Nucl. Instrum. Methods Phys. Res. Sect. A **334**, 305 (1993).
12. B.M. Penetrante, J.N. Bardsley, M.A. Levine, D.A. Knapp, R.E. Marrs, Evaporative cooling of highly charged dysprosium ions in an enhanced electron-beam ion trap. Phys. Rev. A: At. Mol. Opt. Phys. **43**, 4873 (1991)

13. P. Beiersdorfer, V. Decaux, S.R. Elliott, K. Widmann, K. Wong, Temperature of the ions produced and trapped in an electron-beam ion trap. Rev. Sci. Instr. **66**, 303 (1995)
14. B.J. Wargelin, P. Beiersdorfer, S.M. Kahn, Radiative lifetime of the long-lived $1s2s\ ^3S_1$ state in heliumlike neon by electron-beam excitation of trapped ions. Phys. Rev. Lett. **71**, 2196 (1993)
15. P. Beiersdorfer, L. Schweikhard, J.R. Crespo López-Urrutia, K. Widmann, The magnetic trapping mode of an electron beam ion trap: New opportunities for highly charged ion research. Rev. Sci. Instr. **67**, 3818 (1996)
16. J.D. Silver, A.J. Varney, H.S. Margolis, P.E.G. Baird, I.P. Grant, P.D. Groves, W.A. Hallett, A.T. Handford, P.J. Hirst, A.R. Holmes, D.J.H. Howie, R.A. Hunt, K.A. Nobbs, M. Roberts, W. Studholme, J.S. Wark, M.T. Williams, M.A. Levine, D.D. Dietrich, W.G. Graham, I.D. Williams, R. O'Neil, S.J. Rose, The Oxford electron-beam ion trap: A device for spectroscopy of highly charged ions. Rev. Sci. Instr. **65**, 1072 (1994)
17. D.J. Bieber, H.S. Margolis, P.K. Oxley, J.D. Silver, Studies of magnetic dipole transitions in highly charged argon and barium using an electron beam ion trap. Phys. Scr. T **73**, 64–66 (1997)
18. J.D. Gillaspy, EBIT spectra of highly stripped ions from the visible to the X-ray. Phys. Scr. T **65**, 168 (1996)
19. J.D. Gillaspy, Y. Aglitskiy, E. Bell, C.M. Brown, C. Chantler, R.D. Deslattes, U. Feldman, L. Hudson, J.M. Laming, E.S. Meyer, C.A. Morgan, J.R. Roberts, F.G. Serpa, J. Sugar, E. Takacs, First results from the EBIT at NIST. Phys. Scr. T **71**, 99 (1997)
20. F.J. Currell, J. Asada, K. Ishii, A. Minoh, K. Motohashi, N. Nakamura, K. Nishizawa, S. Ohtani, K. Okazaki, M. Sakurai, H. Shiraishi, S. Tsurubuchi, H. Watanabe, A new versatile electron-beam ion trap. J. Phys. Soc. Jpn. **65**, 3186 (1996)
21. H. Watanabe, J. Asada, F.J. Currell, T. Fukami, T. Hirayama, K. Motohashi, N. Nakamura, E. Nojikawa, S. Ohtani, K. Okazaki, M. Sakurai, H. Shimizu, N. Tada, S. Tsurubuchi, Characteristics of the Tokyo electron-beam ion trap. J. Phys. Soc. Jpn. **66**, 3795 (1997)
22. N. Nakamura, J. Asada, F.J. Currell, T. Fukami, T. Hirayama, K. Motohashi, T. Nagata, E. Nojikawa, S. Ohtani, K. Okazaki, M. Sakurai, H. Shiraishi, S. Tsurubuchi, H. Watanabe, An overview of the Tokyo electron beam ion trap. Phys. Scr. T **73**, 362 (1997)
23. H. Khodja, J.P. Briand, A warm electron beam ion trap: the micro-EBIT. Phys. Scr. T **71**, 113 (1997)
24. P. Beiersdorfer, A "brief" history of spectroscopy on EBIT. Can. J. Phys. **86**, 1 (2008)
25. R.E. Marrs, S.R. Elliott, J.H. Scofield, Measurement of electron-impact ionization cross sections for hydrogenlike high-Z ions. Phys. Rev. A: At. Mol. Opt. Phys. **56**, 1338 (1997)
26. P. Beiersdorfer, A.L. Osterheld, V. Decaux, K. Widmann, Observation of lifetime-limited X-ray linewidths in cold highly charged ions. Phys. Rev. Lett. **77**, 5353 (1996)
27. F.G. Serpa, C.A. Morgan, E.S. Meyer, J.D. Gillaspy, E. Träbert, D.A. Church, E. Takács, Measurement of a magnetic-dipole transition probability in Xe^{32+} using an electron-beam ion trap. Phys. Rev. A: At. Mol. Opt. Phys. **55**, 4196 (1997)
28. G.S. Stefanelli, P. Beiersdorfer, V. Decaux, K. Widmann, Measurement of the radiative lifetime of the $1s2s\ ^3S_1$ level in heliumlike magnesium. Phys. Rev. A: At. Mol. Opt. Phys. **52**, 3651 (1995)
29. J.R. Crespo López-Urrutia, P. Beiersdorfer, D.W. Savin, K. Widmann, Precision measurement of the lifetime of the $1s2s\ ^3S_1$ metastable level in heliumlike O^{6+}. Phys. Rev. A: At. Mol. Opt. Phys. **58**, 238 (1998)
30. P. Beiersdorfer, E. Träbert, E.H. Pinnington, Experimental transition rate of the green coronal line of Fe XIV. Astrophys. J. Lett. **587**, 836 (2003)
31. A. Lapierre, U.D. Jentschura, J.R. Crespo, López-Urrutia, J. Braun, G. Brenner, H. Bruhns, D. Fischer, A.J. González Martínez, Z. Harman, W.R. Johnson, C.H. Keitel, V. Mironov, C.J. Osborne, G. Sikler, R. Soria Ort, V. Shabaev, H. Tawara, I.I. Tupitsy, J. Ullrich, A. Volotka, Relativistic electron correlation, quantum electrodynamics, and the lifetime of the $1s^2 2s^2 2p\ ^2P^o_{3/2}$ level in boronlike argon. Phys. Rev. Lett. **95**, 183001 (2005)

32. E. Träbert, P. Beiersdorfer, S.B. Utter, G.V. Brown, H. Chen, C.L. Harris, P.A. Neill, D.W. Savin, A.J. Smith, Experimental M1 transition rates of coronal lines from Ar X, Ar XIV, and Ar XV. Astrophys. J. Lett. **541**, 506 (2000)
33. E. Träbert, S.B. Utter, P. Beiersdorfer, Visible-range spectroscopy and a lifetime measurement on Kr^{22+} in an electron beam ion trap. Phys. Lett. A **272**, 86–92 (2000)
34. E. Träbert, P. Beiersdorfer, G.V. Brown, K. Boyce, R.L. Kelley, C.A. Kilbourne, F.S. Porter, A. Szymkowiak, Time-resolved soft-X-ray spectroscopy of a magnetic octupole transition in nickel-like xenon, cesium, and barium ions. Phys. Rev. A: At. Mol. Opt. Phys. **73**, 022508 (2006)
35. G. Brenner, J.R. Crespo, López-Urrutia, Z. Harman, P.H. Mokler, J. Ullrich, Lifetime determination of the Fe XIV $3s^2 3p\ ^2P_{3/2}$ metastable level. Phys. Rev. A: At. Mol. Opt. Phys. **75**, 032504 (2007)
36. J.D. Gillaspy, Highly charged ions. J. Phys. B: At. Mol. Opt. Phys. **34**, R93 (2001)
37. W.D. Chen, J. Xiao, Y. Shen, Y.Q. Fu, F.C. Meng, C.Y. Chen, B.H. Zhang, Y.J. Tang, R. Hutton, Y. Zou, Precise studies on resonant energies of the first intershell (KLL) dielectronic recombination processes for He- up to O-like xenon. Phys. Plasmas **15**, 083301 (2008)
38. J.R. Crespo López-Urrutia, A. Dorn, R. Moshammer, J. Ullrich, The Freiburg electron beam ion trap/source project FREEBIT. Phys. Scr. T **80**, 502 (1999)
39. S.W. Epp, J.R. Crespo, López-Urrutia, G. Brenner, V. MäckelcKel, P.H. Mokler, R. Treusch, M. Kuhlmann, M.V. Yurkov, J. Feldhaus, J.R. Schneider, M. Wellhöfer, M. Martins, W. Wurth, J. Ullrich, Soft X-ray laser spectroscopy on trapped highly charged ions at FLASH. Phys. Rev. Lett. **98**, 183001 (2007)
40. X. Zhu, Y. Liu, X. Wang, Y. Liu, P. Guo, D. Lu, X. Zhang, W. Hu, M. He, L. Liljeby, Y. Zou, Status of the Shanghai EBIT. Nucl. Instrum. Methods Phys. Res. Sect. B **235**, 509 (2005)
41. S. Böhm, A. Enulescu, T. Fritio, I. Orban, S. Tashenov, R. Schuch, First results from the Stockholm electron beam ion trap. J. Phys: Conf. Ser. **58**, 303 (2007)
42. U. Kentsch, G. Zschornack, F. Gromann, V.P. Ovsyannikov, F. Ullmann, S. Fritzsche, A. Surzhykov, Production of bare argon, manganese, iron and nickel nuclei in the Dresden EBIT. Nucl. Instrum. Methods Phys. Res. Sect. B **187**, 238 (2002)
43. N. Nakamura, A.P. Kavanagh, H. Watanabe, H.A. Sakaue, Y. Li, D. Kato, F.J. Currell, S. Ohtani, Evidence for strong Breit interaction in dielectronic recombination of highly charged heavy ions. Phys. Rev. Lett. **100**, 073203 (2008)
44. N. Nakamura, H. Kikuchi, H.A. Sakaue, T. Watanabe, Compact electron beam ion trap for spectroscopy of moderate charge state ions. Rev. Sci. Instr. **79**, 063104 (2008)
45. M.C. Simon, M. Schwarz, B.L. Schmitt, C. Beilmann, S.W. Epp, T.M. Baumann, K. Kubiček, R. Ginzel, S.G. Higgins, R. Klawitter, V. Mäckel, S. Bernitt, P.H. Mokler, J. Ullrich, J.R. Crespo, López-Urrutia, Photoionization of ions in arbitrary charge states by synchrotron radiation in an electron beam ion trap. J. Phys: Conf. Ser. **194**, 012009 (2009)
46. M.C. Simon, M. Schwarz, S.W. Epp, C. Beilmann, B.L. Schmitt, Z. Harman, T.M. Baumann, P.H. Mokler, S. Bernitt, R. Ginzel, S.G. Higgins, C.H. Keitel, R. Klawitter, K. Kubiček, V. Mäckel, J. Ullrich, J.R. Crespo, López-Urrutia, Photoionization of N^{3+} and Ar^{8+} in an electron beam ion trap by synchrotron radiation. J. Phys. B: At. Mol. Opt. Phys. **43**, 065003 (2010)
47. M.C. Simon, J.R. Crespo López-Urrutia, C. Beilman, M. Schwarz, Z. Harman, S.W. Epp, B.L. Schmitt, T.M. Baumann, E. Behar, S. Bernitt, R. Follath, R. Ginzel, C.H. Keitel, R. Klawitte, K. Kubiček, V. Mäckel, P.H. Mokle, G. Reichardt, O. Schwarzkopf, J. Ullric, Resonant and near-threshold photoionization cross sections of Fe^{14+}. Phys. Rev. Lett. **105**, 183001 (2010)
48. S. Bernitt, G.V. Brown, J.K. Rudolph, R. Steinbrügge, A. Graf, M. Leutenegger, S.W. Epp, S. Eberle, K. Kubiček, V. Mäckel, M.C. Simon, E. Träbert, E.W. Magee, C. Beilmann, N. Hell, S. Schippers, A. Müller, S.M. Kahn, A. Surzhykov, Z. Harman, C.H. Keitel, J. Clementson, F.S. Porter, W. Schlotter, J.J. Turner, J. Ullrich, P. Beiersdorfer, J.R. Crespo, López-Urrutia, An unexpectedly low oscillator strength as the origin of the FeXVII emission problem. Nature **492**, 225 (2012)

49. S. Bernitt, G.V. Brown, J.R. Crespo, López-Urrutia, J. Rudolph, R. Steinbrügge, A. Graf, M. Leutenegger, C. Beilmann, S. Eberle, S.W. Epp, K. Kubiček, V. Mäckel, S. Schippers, W. Schlotter, M.C. Simon, E. Träbert, J. Turner, S.M. Kahn, E.W. Magee, A. Müller, F.S. Porter, A. Rasmussen, P. Beiersdorfer, J. Ullrich, X-ray laser spectroscopy with an electron beam ion trap at the free electron laser LCLS. J. Phys: Conf. Ser. **388**, 032037 (2012)
50. P. Beiersdorfer, Laboratory X-ray astrophysics. Ann. Rev. Astron. Astrophys. **41**, 343 (2003)
51. S.B. Utter, P. Beiersdorfer, J.R. Crespo López-Urrutia, K. Widmann, Position and size of the electron beam in the high-energy electron beam ion trap. Nucl. Instrum. Methods Phys. Res. Sect. A **428**, 276 (1999)
52. B. O'Rourke, F.J. Currell, H. Kuramoto, Y.M. Li, S. Ohtani, X.M. Tong, H. Watanabe, Electron-impact ionization of hydrogen-like iron ions. J. Phys. B: At. Mol. Opt. Phys. **34**, 4003 (2001)
53. H. Watanabe, F.J. Currell, H. Kuramoto, S. Ohtani, B.E. O'Rourke, X.M. Tong, Electron impact ionization of hydrogen-like molybdenum ions. J. Phys. B: At. Mol. Opt. Phys. **35**, 5095 (2002)
54. P. Beiersdorfer, V. Decaux, K. Widmann, Measurement of the temperature of cold highly charged ions produced in an electron beam ion trap. Nucl. Instrum. Methods Phys. Res. Sect. A **98**, 566 (1995)
55. L. Schweikhard, P. Beiersdorfer, G.V. Brown, J.R. Crespo López-Urrutia, S.B. Utter, K. Widmann, Pulsed gas injection for X-ray spectroscopy of highly charged ions stored in the magnetic trapping mode of an electron beam ion trap. Nucl. Instrum. Methods Phys. Res. Sect. A **142**, 245 (1998)
56. P. Beiersdorfer, K.R. Boyce, G.V. Brown, H. Chen, S.M. Kahn, R.L. Kelley, M. May, R.E. Olson, F.S. Porter, C.K. Stahle, W.A. Tillotson, Laboratory simulation of charge exchange–produced X-ray emission from comets. Science **300**, 1558 (2003)
57. W. Lotz, An empirical formula for the electron-impact ionization cross-section. Zeitschrift für Physik **206**, 205 (1967)
58. H.A. Bethe, E.E. Salpeter, *Quantum Mechanics of One- and Two-Electron Atoms* (Springer, Berlin, 1957)
59. H. van Regemorter, Rate of collisional excitation in stellar atmospheres. Astrophys. J. **136**, 906 (1962)
60. E.E. Salpeter, H.A. Bethe, A relativistic equation for bound-state problems. Phys. Rev. **84**, 1232 (1951)
61. M.F. Gu, The flexible atomic code. Can. J. Phys. **86**, 675 (2008)
62. S. Fritzsche, The RATIP program for relativistic calculations of atomic transition, ionization and recombination properties. Comput. Phys. Commun. **183**(7), 1525 (2012)
63. A.J. González Martínez, J.R. Crespo López-Urrutia, J. Braun, G.Brenner, H. Bruhns, A. Lapierre, V. Mironov, R. Soria Orts, H. Tawara, M. Trinczek, J. Ullrich, J.H. Scofield, State-selective quantum interference observed in the recombination of highly charged $Hg^{75+...78+}$ mercury ions in an electron beam ion trap. Phys. Rev. Lett. **94**, 203201 (2005)
64. P. Beiersdorfer, R.E. Marrs, J.R. Henderson, D.A. Knapp, M.A. Levine, D.B. Platt, M.B. Schneider, D.A. Vogel, K.L. Wong, High-resolution x-ray spectrometer for an electron beam ion trap. Rev. Sci. Instrum. **61**, 2338 (1990)
65. J.W.M. DuMond, A high resolving power, curved-crystal focusing spectrometer for the short wave-length x-rays and gamma-rays. Rev. Sci. Instrum. **18**, 626 (1947)
66. H.H. Johann, Die Erzeugung lichtstarker Röntgenspektren mit Hilfe von Konkavkristallen. Zeitschrift für Physik **69**, 185 (1931)
67. P. Beiersdorfer, B.J. Wargelin, Low energy x-ray spectrometer for an electron beam ion trap. Rev. Sci. Instrum. **65**, 13 (1994)
68. P. Beiersdorfer, J.R. Crespo, López-Urrutia, E. Förster, J. Mahiri, K. Widmann, Very high resolution soft x-ray spectrometer for an electron beam ion trap. Revi. Sci. Instrum. **68**, 1077 (1997)
69. P. Beiersdorfer, J.R. Crespo, López-Urrutia, P. Springer, S.B. Utter, K.L. Wong, Spectroscopy in the extreme ultraviolet on an electron beam ion trap. Rev. Sci. Instrum. **70**, 276 (1999)

70. G.V. Brown, P. Beiersdorfer, K. Widmann, Wide-band, high-resolution soft x-ray spectrometer for the electron beam ion trap. Rev. Sci. Instrum. **70**, 280 (1999)
71. S.B. Utter, G.V. Brown, P. Beiersdorfer, E.J. Clothiaux, N.K. Podder, Grazing-incidence measurements of L-shell line emission from highly charged Fe in the soft x-ray region. Rev. Sci. Instrum. **70**, 284 (1999)
72. C. Biedermann, R. Radtke, J.-L. Schwob, P. Mandelbaum, R. Doron, T. Fuchs, G. Fußmann, EUV spectroscopy of highly charged tungsten ions relevant to hot plasmas. Phys. Scr. T **92**, 85 (2001)
73. P. Beiersdorfer, E.W. Magee, E. Träbert, H. Chen, J.K. Lepson, M.-F. Gu, M. Schmidt, Flat-field grating spectrometer for high-resolution soft x-ray and extreme ultraviolet measurements on an electron beam ion trap. Rev. Sci. Instrum. **75**, 3723 (2004)
74. F.S. Porter, G.V. Brown, K.R. Boyce, R.L. Kelley, C.A. Kilbourne, P. Beiersdorfer, H. Chen, S. Terracol, S.M. Kahn, A.E. Szymkowiak, The astro-e2 x-ray spectrometer/EBIT microcalorimeter x-ray spectrometer. Rev. Sci. Instrum. **75**, 3772 (2004)
75. M.I. Eides, H. Grotch, V.A. Shelyuto, Theory of light hydrogenlike atoms. Phys. Rep. **342**, 63 (2001)
76. K. Pachucki, Higher-order binding corrections to the Lamb shift. Ann. Phys. **226**(1), 1 (1993)
77. P.J. Mohr, Self-energy radiative corrections in hydrogen-like systems. Ann. Phys. **88**, 26 (1974)
78. P.J. Mohr, Quantum electrodynamics of high-Z few-electron atoms. Phys. Rev. A: At. Mol. Opt. Phys. **32**, 1949 (1985)
79. W.R. Johnson, G. Soff, The Lamb shift in hydrogen-like atoms, $1 < Z < 110$. At. Data Nucl. Data Tables **33**, 405 (1985)
80. P.J. Mohr, Self-energy correction to one-electron energy levels in a strong Coulomb field. Phys. Rev. A: At. Mol. Opt. Phys. **46**, 4421 (1992)
81. P.J. Mohr, G. Soff, Nuclear size correction to the electron self-energy. Phys. Rev. Lett. **70**, 158 (1993)
82. P.J. Mohr, G. Plunien, G. Soff, QED corrections in heavy atoms. Phys. Rep. **293**, 227 (1998)
83. V.M. Shabaev, A.N. Artemyev, V.A. Yerokhin, QED and nuclear effects in high-Z few-electron atoms. Phys. Scr. T **86**, 7 (2000)
84. V.M. Shabaev, Two-time Green's function method in quantum electrodynamics of high-Z few-electron atoms. Phys. Rep. **356**, 119 (2002)
85. J.L. Flowers, H.A. Klein, D.J. E. Knight, H.S. Margolis, Hydrogenic systems for calculable frequency standards: Status and options. NPL Report CBTLM 11, March 2001
86. R. Deslattes, E.G. Kessler, X-ray transition energies: new approach to a comprehensive evaluation. Rev. Mod. Phys. **75**, 35 (2003)
87. V.A. Yerokhin, P. Indelicato, V.M. Shabaev, Two-loop self-energy correction in high-Z hydrogenlike ions. Phys. Rev. Lett. **91**, 073001 (2003)
88. V.M. Shabaev, Finite nuclear size corrections to the energy levels of the multichargedions. J. Phys. B: At. Mol. Opt. Phys. **26**, 1103 (1993)
89. V.M. Shabaev, Mass corrections in a strong nuclear field. Theor. Math. Phys. **63**, 588 (1985)
90. A.N. Artemyev, V.M. Shabaev, V.A. Yerokhin, Relativistic nuclear recoil corrections to the energy levels of hydrogenlike and high-Z lithiumlike atoms in all orders in αZ. Phys. Rev. A: At. Mol. Opt. Phys. **52**, 1884 (1995)
91. G. Plunien, B. Müller, W. Greiner, G. Soff, Nuclear polarization contribution to the Lamb shift in heavy atoms. Phys. Rev. A: At. Mol. Opt. Phys. **39**, 5429 (1989)
92. J.P. Briand, M. Tavernier, P. Indelicato, R. Marrus, H. Gould, High-precision spectroscopic studies of Lyman-α lines of hydrogenlike iron: A measurement of the 1s Lamb shift. Phys. Rev. Lett. **50**, 832 (1983)
93. J.P. Briand, M. Tavernier, R. Marrus, J.P. Desclaux, High-precision spectroscopic study of heliumlike iron. Phys. Rev. A: At. Mol. Opt. Phys. **29**, 3143 (1984)
94. E. Källne, J. Källne, P. Richard, M. Stöckli, Precision measurement of the H-like x-ray spectrum of Cl and the 1s Lamb shift. J. Phys. B: At. Mol. Opt. Phys. **17**, L115 (1984)

95. P. Richard, M. Stöckli, R.D. Deslattes, P. Cowan, R.E. LaVilla, B. Johnson, K. Jones, M. Meron, R. Mann, K. Schartner, Measurement of the 1*s* Lamb shift in hydrogenlike chlorine. Phys. Rev. A: At. Mol. Opt. Phys. **29**, 2939 (1984)
96. M. Tavernier, J.P. Briand, P. Indelicato, D. Liesen, P. Richard, Measurement of the (1s) Lamb shift of hydrogen-like krypton. J. Phys. B: At. Mol. Opt. Phys. **18**, L327–L330 (1985)
97. E.S. Marmar, J.E. Rice, E. Källne, J. Källne, R.E. LaVilla, Precision measurement of the 1*s* Lamb shift in hydrogenlike argon. Phys. Rev. A: At. Mol. Opt. Phys. **33**, 774 (1986)
98. R.D. Deslattes, H.F. Beyer, F. Folkmann, Precision x-ray wavelength measurements in helium-like argon recoil ions. J. Phys. B: At. Mol. Opt. Phys. **17**, L689 (1984)
99. H.F. Beyer, R.D. Deslattes, F. Folkmann, R.E. LaVilla, Determination of the 1s Lamb shift in one-electron argon recoil ions. J. Phys. B: At. Mol. Opt. Phys. **18**, 207–215 (1985)
100. H.F. Beyer, P. Indelicato, K.D. Finlayson, D. Liesen, R.D. Deslattes, Measurement of the 1s Lamb shift in hydrogenlike nickel. Phys. Rev. A: At. Mol. Opt. Phys. **43**, 223 (1991)
101. R.D. Deslattes, R. Schuch, E. Justiniano, Application of decelerated bare nuclei to precision spectroscopy of one-electron ions. Phys. Rev. A: At. Mol. Opt. Phys. **32**, 1911 (1985)
102. G. Hölzer, E. Förster, D. Klöpfel, P. Beiersdorfer, G.V. Brown, J.R. Crespo, López-Urrutia, K. Widmann, Absolute wavelength measurement of the Lyman-α transitions of hydrogenic Mg^{11+}. Phys. Rev. A: At. Mol. Opt. Phys. **57**, 945 (1998)
103. D. Klöpfel, G. Hölzer, E. Förster, P. Beiersdörfer, A quartz quasimonolith for absolute x-ray wavelength measurements. Rev. Sci. Instrum. **68**, 3669 (1997)
104. J. Tschischgale, D. Klöpfel, P. Beiersdorfer, G.V. Brown, E. Förster, H. Schulte-Schrepping, S.B. Utter, Absolute wavelength measurement of the Lyman-α transition of hydrogen-like silicon. Can. J. Phys. **80**, 867 (2002)
105. J.D. Gillaspy, C.T. Chantler, D. Paterson, L.T. Hudson, F.G. Serpa, E. Takcs, First measurement of Lyman-α x-ray lines in hydrogen-like vanadium: Results and implications for precision wavelength metrology and tests of QED. J. Phys. B: At. Mol. Opt. Phys. **43**, 074021 (2010)
106. N. Nakamura, D. Kato, N. Miura, T. Nakahara, S. Ohtani, Intensity ratio between Lyman-α1 and Lyman-α2 lines of hydrogenlike titanium observed in an electron-beam ion trap. Phys. Rev. A: At. Mol. Opt. Phys. **63**, 024501 (2001)
107. M.R. Tarbutt, R. Barnsley, N.J. Peacock, J.D. Silver, Wavelength measurements of the satellite transitions to the n = 2 resonance lines of helium-like argon. J. Phys. B: At. Mol. Opt. Phys. **34**, 3979 (2001)
108. W.L. Bond, Precision lattice constant determination. Acta Crystallogr. **13**, 814 (1960)
109. P. Becker, K. Dorenwendt, G. Ebeling, R. Lauer, W. Lucas, R. Probst, H.J. Rademacheer, G. Reim, P. Seyfried, H. Siegert, Absolute measurement of the (220) lattice plane spacing in a silicon crystal. Phys. Rev. Lett. **46**, 1540–1543 (1981)
110. Johannes Braun, *"Entwicklung eines Kristallspektrometers für röntgenspektroskopische Untersuchungen an Hochgeladenen Ionen* (Universität Heidelberg, Master's thesis, 2003)
111. J. Braun, H. Bruhns, M. Trinczek, J.R. Crespo, López-Urrutia, J. Ullrich, Novel technique for high-precision Bragg-angle determination in crystal x-ray spectroscopy. Rev. Sci. Instrum. **76**, 073105 (2005)
112. J. Braun, *Präzisionsröntgenspektroskopie zur absoluten Wellenlängenbestimmung an hochgeladenen Ionen* (Diss, Max-Planck-Institut für Kernphysik, 2006)
113. H. Bruhns, High-precision x-ray spectroscopy on highly charged argon ions. PhD thesis, Universität Heidelberg, Germany, Dezember 2005
114. H. Bruhns, J. Braun, K. Kubiček, J.R. Crespo, López-Urrutia, J. Ullrich, Testing QED screening and two-loop conributions with He-like ions. Phys. Rev. Lett. **99**, 113001 (2007)
115. K. Kubiček, *Absolute determination of the* $n = 1$ *to* $n = 2$ *transition energies in hydrogen- and helium-like* S^{14+}, S^{15+}, Ar^{16+} *and* Ar^{17+} *ions* (Universität Göttingen, Master's thesis, 2006)
116. K. Kubiček, H. Bruhns, J. Braun, J.R. Crespo, López-Urrutia, J. Ullrich, Two-loop QED contributions tests with mid-*Z* He-like ions. J. Phys: Conf. Ser. **163**, 012007 (2009)
117. K. Kubiček, J. Braun, H. Bruhns, J.R. Crespo, López-Urrutia, P. H. Mokler, J. Ullrich, High-precision laser-assisted absolute determination of x-ray diffraction angles. Rev. Sci. Instrum. **83**, 013102 (2012)

118. D.R. Plante, W.R. Johnson, J. Sapirstein, Relativistic all-order many-body calculations of the n=1 and n=2 states of heliumlike ions. Phys. Rev. A: At. Mol. Opt. Phys. **49**, 3519 (1994)
119. K.G. Dyall, I.P. Grant, C.T. Johnson, F.A. Parpia, E.P. Plummer, Grasp: A general-purpose relativistic atomic structure program. Comput. Phys. Commun. **55**, 425 (1989)
120. P. Indelicato, O. Gorceix, M. Tavernier, J.P. Briand, J.P. Desclaux, R. Marrus, M. Prior, Experimental and theoretical study of QED corrections in the ground state of heliumlike iron. Zeitschrift für Physik D: At. Mol. Clusters **2**, 149 (1986)
121. P. Indelicato, O. Gorveix, J.P. Desclaux, Multiconfiguration Dirac-Fock studies of two-electron ions: II. Radiative corrections and comparison with experiment. J. Phys. B: At. Mol. Opt. Phys. **20**, 651 (1987)
122. K.T. Cheng, M.H. Chen, W.R. Johnson, J. Sapirstein, Relativistic configuration-interaction calculations for the ground state and $n = 2$ singlet states in heliumlike ions. Phys. Rev. A: At. Mol. Opt. Phys. **50**, 247 (1994)
123. K.T. Cheng, M.H. Chen, Energy levels of the low-lying states of mid-Z heliumlike ions. Phys. Rev. A: At. Mol. Opt. Phys. **61**, 044503 (2000)
124. G.W.F. Drake, Theoretical energies for the n=1 and 2 states of the helium isoelectronic sequence up to Z=100. Can. J. Phys. **66**, 586 (1988)
125. Z.-C. Yan, G.W.F. Drake, High precision calculation of fine structure splittings in helium and He-like ions. Phys. Rev. Lett. **74**, 4791 (1995)
126. G.W.F. Drake, Progress in helium fine-structure calculations and the fine-structure constant. Can. J. Phys. **80**, 1195–1212 (2002)
127. I. Lindgren, H. Persson, S. Salomonson, Full QED calculations of two-photon exchange for heliumlike-systems: Analysisin the Coulomb and Feynman gauges. Phys. Rev. A: At. Mol. Opt. Phys. **51**, 1167 (1995)
128. I. Lindgren, B. Asen, S. Salomonson, A.M. Mårtensson-Pendrill, QED procedure applied to the quasidegenerate fine-structure levels of He-like ions. Phys. Rev A: At. Mol. Opt. Phys. **64**, 062505 (2001)
129. W.R. Johnson, K.T. Cheng, M.H. Chen, Chapter 3: Accurate relativistic calculations including QED contributions for few-electron systems. Theor. Comput. Chem. **14**, 120 (2004)
130. J. Sapirstein, K.T. Cheng, M.H. Chen, Potential independence of the solution to the relativistic many-body problem and the role of negative-energy states in heliumlike ions. Phys. Rev. A: At. Mol. Opt. Phys. **59**, 259 (1999)
131. A.N. Artemyev, V.M. Shabaev, V.A. Yerokhin, G. Plunien, G. Stoff, QED calculation of the n = 1 and n = 2 energy levels in He-like ions. Phys. Rev. A: At. Mol. Opt. Phys. **71**, 062104 (2005)
132. O.Y. Andreev, L.N. Labozowsky, G. Plunien, G. Stoff, Calculation of quasidegenerate energy levels of two-electron ions. Phys. Rev. A: At. Mol. Opt. Phys. 69 (2004)
133. L. Schleinkofer, F. Bell, H.-D. Betz, G. Trollmann, J. Rothermel, Precision wavelength determination of $2^1P_1 - 1^1S_0$ and $2^3P_1 - 1^1S_0$ transitions in helium-like sulfur ions. Phys. Scr. **25**, 917 (1982)
134. E.V. Aglitsky, P.S. Antisiferov, S.L. Mandelstam, A.M. Panin, U.I. Safronova, S.A. Ulitin, Comparison of calculated and measured wavelengths of resonance transitions in He-like ions for Z=16-39. Phys. Scr. **38**, 136 (1988)
135. P. Beiersdorfer, M. Bitter, S. von Goeler, K.W. Hill, Experimental study of the x-ray transitions in the heliumlike isoelectronic sequence. Phys. Rev. A: At. Mol. Opt. Phys. **40**, 150 (1989)
136. C. Biedermann, R. Radtke, K.B. Fournier, Spectroscopy of heliumlike argon resonance and satellite lines for plasma temperature diagnostics. Phys. Rev. E: Stat. Nonlin. Soft Matter Phys. **66**, 066404 (2002)
137. C.T. Chantler, D. Paterson, L.T. Hudson, F.G. Serpa, J.D. Gillaspy, E. Takács, Absolute measurement of the resonance lines in heliumlike vanadium on an electron-beam ion trap. Phys. Rev. A: At. Mol. Opt. Phys. **62**, 042501 (2000)
138. H. Bruhns, J. Braun, K. Kubiček, J.R. Crespo, López-Urrutia, J. Ullrich, Testing QED screening and two-loop contributions with He-like ions. Phys. Rev. Lett. **99**, 113001 (2007)

139. C.T. Chantler, J.M. Laming, D.D. Dietrich, W.A. Hallett, R. McDonald, J.D. Silver, Hydrogenic Lamb shift in iron Fe^{25+} and fine-structure Lamb shift. Phys. Rev. A: At. Mol. Opt. Phys. **76**, 042116 (2007)
140. J.K. Rudolph, J.R. Crespo López-Urrutia, et al., X-Ray Resonant Photoexcitation: Linewidths and Energies of $K\alpha$ Transitions in Highly Charged Fe Ions. Phys. Rev. Lett. **111**(10), 103002 (2013)
141. V.A. Yerokhin, A. Surzhykov, Relativistic configuration-interaction calculation of energy levels of core-excited states in lithiumlike ions: Argon through krypton. Phys. Rev. A: At. Mol. Opt. Phys. **86**, 042507 (2012)
142. U. Staude, Ph. Bosselmann, R. Büttner, D. Horn, K.-H. Schartner, F. Folkmann, A.E. Livingston, T. Ludziejewski, P.H. Mokler, Measurements of $2s\ ^2S_{1/2}$–$2p\ ^2P_{3/2,1/2}$ transition energies in lithiumlike heavy ions: Experiments and results for Ni^{25+} and Zn^{27+}. Phys. Rev. A: At. Mol. Opt. Phys. **58**, 3516 (1998)
143. Ph Bosselmann, U. Staude, D. Horn, K.-H. Schartner, F. Folkmann, A.E. Livingston, P.H. Mokler, Measurements of $2s\ ^2S_{1/2}$–$2p\ ^2P_{3/2,1/2}$ transition energies in lithiumlike heavy ions. II. experimental results for Ag and discussion along the isoelectronic series. Phys. Rev. A: At. Mol. Opt. Phys. **59**, 1874 (1999)
144. D. Feili, Ph Bosselmann, K.-H. Schartner, F. Folkmann, A.E. Livingston, E. Träbert, X. Ma, P.H. Mokler, Measurements of $2s\ ^2S_{1/2}$–$2p\ ^2P_{1/2}$ transition energies in lithiumlike heavy ions. III. experimental results for Sn^{47+} and Xe^{51+}. Phys. Rev. A: At. Mol. Opt. Phys. **62**, 022501 (2000)
145. C. Brandau, T. Bartsch, A. Hoffknecht, H. Knopp, S. Schippers, W. Shi, A. Müller, N. Grün, W. Scheid, T. Steih, F. Bosch, B. Franzke, C. Kozhuharov, P.H. Mokler, F. Nolden, M. Steck, T. Stöhlker, Z. Stachura, High Rydberg resonances in dielectronic recombination of Pb^{79+}. Phys. Rev. Lett. **89**, 053201 (2002)
146. C. Brandau, C. Kozhuharov, A. Müller, W. Shi, S. Schippers, T. Bartsch, S. Böhm, C. Böhme, A. Hoffknecht, K. Knopp, N. Grün, W. Scheid, T. Steih, F. Bosch, B. Franzke, P.H. Mokler, F. Nolden, T. Stöhlker, Z. Stachura, Precise determination of the $2s_{1/2} - 2p_{1/2}$ splitting in very heavy lithiumlike ions utilizing dielectronic recombination. Phys. Rev. Lett. **91**, 073202 (2003)
147. P. Beiersdorfer, D. Knapp, R.E. Marrs, S.R. Elliott, M.H. Chen, Structure and Lamb shift of $2s_{1/2}$–$2p_{1/2}$ levels in lithiumlike U^{89+} through neonlike U^{82+}. Phys. Rev. Lett. **71**, 3939 (1993)
148. S.A. Blundell, Accurate screened QED calculations in high-Z many-electron ions. Phys. Rev. A: At. Mol. Opt. Phys. **46**, 3762 (1992)
149. P. Beiersdorfer, A. Osterheld, S.R. Elliott, M.H. Chen, D. Knapp, K. Reed, Structure and lamb shift of $2s_{1/2}$–$2p_{3/2}$ levels in lithiumlike Th^{87+} through neonlike Th^{80+}. Phys. Rev. A: At. Mol. Opt. Phys. **52**, 2693 (1995)
150. P. Beiersdorfer, A.L. Osterheld, J.H. Scofield, J.R. Crespo, López-Urrutia, K. Widmann, Measurement of QED and hyperfine splitting in the $2s_{1/2}$–$2p_{3/2}$ x-ray transition in Li-like $^{209}Bi^{80+}$. Phys. Rev. Lett. **80**, 3022 (1998)
151. Y. Podpaly, J. Clementson, P. Beiersdorfer, J. Williamson, G.V. Brown, M.F. Gu, Spectroscopy of $2s_{1/2}$–$2p_{3/2}$ transitions in W^{65+} through W^{71+}. Phys. Rev. A: At. Mol. Opt. Phys. **80**, 052504 (2009)
152. Y.-K. Kim, D.H. Baik, P. Indelicato, J.P. Desclaux, Resonance transition energies of Li-, Na-, and Cu-like ions. Phys. Rev. A: At. Mol. Opt. Phys. **44**, 148 (1991)
153. P. Beiersdorfer, Testing QED and atomic-nuclear interactions with high-Z ions. J. Phys. B: At. Mol. Opt. Phys. **43**, 074032 (2010)
154. P. Beiersdorfer, H. Chen, D.B. Thorn, E. Träbert, Measurement of the two-loop Lamb shift in lithiumlike U^{89+}. Phys. Rev. Lett. **95**, 233003 (2005)
155. A.N. Artemyev, V.M. Shabaev, M.M. Sysak, V.A. Yerokhin, T. Beierand, G. Plunien, G. Soff, Evaluation of the two-photon exchange diagrams for the $(1s)^2 2p_{3/2}$ electron configuration in Li-like ions. Phys. Rev. A: At. Mol. Opt. Phys. **67**, 062506 (2003)

156. P. Beiersdorfer, E. Träbert, H. Chen, M.-H. Chen, M.J. May, A.L. Osterheld, Measurement of the $3s_{1/2}$–$3p_{3/2}$ resonance line in Na-like U^{81+}. Phys. Rev. A: At. Mol. Opt. Phys. **67**, 052103 (2003)
157. X. Zhang, N. Nakamura, Ch. Chen, M. Andersson, Y. Liu, Sh Ohtani, Measurement of the QED energy shift in the $1s^2 2p_{3/2} 1s^2 2s_{1/2}$ x-ray transition in Li-like $^{208}Pb^{79+}$. Phys. Rev. A: At. Mol. Opt. Phys. **78**, 032504 (2008)
158. C.A. Morgan, F.G. Serpa, E. Takcs, E.S. Meyer, J.D. Gillaspy, J. Sugar, J.R. Roberts, C.M. Brown, U. Feldman, Observation of visible and UV magnetic dipole transitions in highly charged xenon and barium. Phys. Rev. Lett. **74**, 1716 (1995)
159. J.V. Porto, I. Kink, J.D. Gillaspy, UV light from the ground term of Ti-like ytterbium, tungsten, and bismuth. Phys. Rev. A: At. Mol. Opt. Phys. **61**, 545011 (2000)
160. F.G. Serpa, E.W. Bell, E.S. Meyer, J.D. Gillaspy, J.R. Roberts, Kr spectra from an electron-beam ion trap: 300 nm to 460 nm. Phys. Rev. A: At. Mol. Opt. Phys. **55**, 1832 (1997)
161. H. Watanabe, D. Crosby, F.J. Currell, T. Fukami, D. Kato, S. Ohtani, J.D. Silver, C. Yamada, Magnetic dipole transitions in titaniumlike ions. Phys. Rev. A: At. Mol. Opt. Phys. **63**, 425131–425136 (2001)
162. S.B. Utter, P. Beiersdorfer, G.V. Brown, Measurement of an unusual M1 transition in the ground state of Ti-like W^{52+}. Phys. Rev. A: At. Mol. Opt. Phys. **61**, 305031 (2000)
163. J.R. Crespo López-Urrutia, P. Beiersdorfer, K. Widmann, V. Decaux, Visible spectrum of highly charged ions: The forbidden optical lines of Kr, Xe, Ba ions in the Ar I to Ni I isoelectronic sequence. Phys. Scr. T **80**, 448 (1999)
164. J. R. Crespo López-Urrutia, P. Beiersdorfer, K. Widmann, V. Decaux, Visible spectrum of highly charged ions: The forbidden optical lines of Kr, Xe, and Ba ions in the Ar I to Kr I isoelectronic sequence. Can. J. Phys. **80**, 1687 (2002)
165. I. Draganič, J.R. Crespo, López-Urrutia, R. DuBois, S. Fritzsche, V.M. Shabaev, R. Soria Orts, I.I. Tupitsyn, Y. Zou, J. Ullrich, High precision wavelength measurements of QED-sensitive forbidden transitions in highly charged argon ions. Phys. Rev. Lett. **91**, 1830011 (2003)
166. R.S. Soria Orts, Z. Harman, J.R. Crespo López-Urrutia, A.N. Artemyev, H. Bruhns, A.J. González Martínez, U.D. Jentschura, C.H. Keitel, A. Lapierre, V. Mironov, V.M. Shabaev, H. Tawara, I.I. Tupitsyn, J. Ullrich, A.V. Volotka, Exploring relativistic many-body recoil effects in highly charged ions. Phys. Rev. Lett. **97**, 103002 (2006)
167. C.W.P. Palmer, Reformulation of the theory of the mass shift. J. Phys. B: At. Mol. Phys. **20**, 5987 (1987)
168. R. Soria Orts, J.R. Crespo López-Urrutia, H. Bruhns, A.J. González Martínez, Z. Harman, U.D. Jentschura, C.H. Keitel, A. Lapierre, H. Tawara, I.I. Tupitsyn, J. Ullrich, A.V. Volotka, Zeeman splitting and g factor of the $1s^2 2s^2 2p^2 P_{3/2}$ and $^2P_{1/2}$ levels in Ar^{13+}. Phys. Rev. A: At. Mol. Opt. Phys. **76**, 052501 (2007)
169. J.R. Crespo, López-Urrutia, The visible spectrum of highly charged ions: A window to fundamental physics. Can. J. Phys. **86**, 111 (2008)
170. A. Lapierre, J.R. Crespo, López-Urrutia, J. Braun, G. Brenner, H. Bruhns, D. Fischer, A. J. González Martínez, V. Mironov, C. Osborne, G. Sikler, R. Soria Orts, H. Tawara, J. Ullrich, V. M. Shabaev, I. I. Tupitsyn, A. Volotka, Lifetime measurement of the Ar XIV $1s^2 2s^2 2p\ ^2P^o_{3/2}$ metastable level at the Heidelberg electron-beam ion trap. Phys. Rev. A: At. Mol. Opt. Phys. **73**, 052507 (2006)
171. J.R. Crespo López-Urrutia, B. Bapat, I. Draganič, B. Feuerstein, D. Fischer, H. Lörch, R. Moshammer, J. Ullrich, R.D. Dubois, Y. Zou, Physics with highly-charged ions in an EBIT. Hyperfine Interact. **146**, 109 (2003)
172. F.G. Serpa, J.D. Gillaspy, E. Träbert, Lifetime measurements in the ground configuration of Ar^{13+} and Kr^{22+} using an electron beam ion trap. J. Phys. B: At. Mol. Opt. Phys. **31**, 3345 (1998)
173. D.P. Moehs, D.A. Church, Magnetic dipole transition rates from measured lifetimes of levels of Be-like and B-like argon ions. Phys. Rev. A: At. Mol. Opt. Phys. **58**, 1111 (1998)
174. E. Träbert, Precise atomic lifetime measurements with stored ion beams and ion traps. Can. J. Phys. **80**, 1481 (2002)

175. I.I. Tupitsyn, A.V. Volotka, D.A. Glazov, V.M. Shabaev, G. Plunien, J.R. Crespo, López-Urrutia, A. Lapierre, J. Ullrich, Magnetic-dipole transition probabilities in B-like and Be-like ions. Phys. Rev. A: At. Mol. Opt. Phys. **72**, 062503 (2005)
176. A.N. Artemyev, V.M. Shabaev, I.I. Tupitsyn, G. Plunien, V.A. Yerokhin, QED calculation of the $2p_{3/2}$-$2p_{1/2}$ transition energy in boronlike argon. Phys. Rev. Lett. **98**, 173004 (2007)
177. K.T. Cheng, Y.K. Kim, J.P. Desclaux, Electric dipole, quadrupole, and magnetic dipole transition probabilities of ions isoelectronic to the first-row atoms, Li through F. At. Data Nucl. Data Tables **24**, 111 (1979)
178. C. Froese-Fischer, Multiconfiguration Hartree-Fock Breit-Pauli results for $2p_{1/2}$–$2p_{3/2}$ transitions in the boron sequence. J. Phys. B: At. Mol. Opt. Phys. **16**, 157 (1983)
179. B. Warner, Transition probabilities in *np* and np^5configurations. Zeitschrift für Astrophysik **69**, 399 (1968)
180. M.E. Galavís, C. Mendoza, C.J. Zeippen, Atomic data from the iron project. Astron. Astrophys. Suppl. **133**, 245 (1998)
181. E. Charro, S. López-Ferrero, I. Martín, Forbidden emission coefficients for intraconfiguration transitions $2p_{3/2} \rightarrow 2p_{1/2}$ along the boron sequence. J. Phys. B: At. Mol. Opt. Phys. **34**, 4243 (2001)
182. T.R. Verhey, B.P. Das, W.F. Perger, Multiconfiguration Dirac-Fock calculation of the forbidden $2p_{1/2}$–$2p_{3/2}$ ground-state M1 transition in the boron isoelectronic sequence. J. Phys. B: At. Mol. Opt. Phys. **20**, 3639 (1987)
183. Z. Harman, U.D. Jentschura, C.H. Keitel, A. Lapierre, R.S. Orts, J.R. Crespo, López-Urrutia, H. Tawara, J. Ullrich, A.N. Artemyev, I.I. Tupitsyn, A.V. Volotka, V.M. Shabaev, Correlation and quantum electrodynamic effects on the radiative lifetime and relativistic nuclear recoil in Ar^{13+} and Ar^{14+} ions. J. Phys: Conf. Ser. **58**, 133 (2007)
184. V.M. Shabaev, QED theory of the nuclear recoil effect in atoms. Phys. Rev. A: At. Mol. Opt. Phys. **57**, 59 (1998)
185. I.I. Tupitsyn, V.M. Shabaev, J.R. Crespo, López-Urrutia, I. Draganič, R. Soria Orts, J. Ullrich, Relativistic calculations of isotope shifts in highly charged ions. Phys. Rev. A: At. Mol. Opt. Phys. **68**, 225111 (2003)
186. A.N. Artemyev, V.M. Shabaev, V.A. Yerokhin, Nuclear recoil corrections to the $2p_{3/2}$ state energy of hydrogen-like and high-Z lithium-like atoms in all orders in αZ. J. Phys. B: At. Mol. Opt. Phys. **28**, 5201 (1995)
187. V.M. Shabaev, Hyperfine structure of hydrogen-like ions. J. Phys. B: At. Mol. Opt. Phys. **27**, 5825 (1994)
188. I. Klaft, S. Borneis, T. Engel, B. Fricke, R. Grieser, G. Huber, T. Kühl, D. Marx, R. Neumann, S. Schröder, P. Seelig, L. Völker, Precision laser spectroscopy of the ground state hyperfine splitting of hydrogenlike $^{209}Bi^{82+}$. Phys. Rev. Lett. **73**, 2425 (1994)
189. J.R. Crespo López-Urrutia, P. Beiersdorfer, D.W. Savin, K. Widmann, Direct observation of the spontaneous emission of the hyperfine transition $F = 4$ to $F = 3$ in ground state hydrogenlike $^{165}Ho^{66+}$ in an electron beam ion trap. Phys. Rev. Lett. **77**, 826 (1996)
190. J.R. Crespo López-Urrutia, P. Beiersdorfer, K. Widmann, B.B. Birkett, A.-M. Mårtensson-Pendrill, M.G.H. Gustavsson, Nuclear magnetization distribution radii determined by hyperfine transitions in the 1s level of H-like ions $^{185}Re^{74+}$ and $^{187}Re^{74+}$. Phys. Rev. A: At. Mol. Opt. Phys. **57**, 879 (1998)
191. P. Beiersdorfer, S.B. Utter, K.L. Wong, J.R. Crespo, López-Urrutia, J.A. Britten, H. Chen, C.L. Harris, R.S. Thoe, D.B. Thorn, E. Träbert, M.G.H. Gustavsson, C. Forssén, A.-M. Mårtensson-Pendrill, Hyperfine structure of hydrogenlike thallium isotopes. Phys. Rev. A: At. Mol. Opt. Phys. **64**, 032506 (2001)
192. P. Seelig, S. Borneis, A. Dax, T. Engel, S. Faber, M. Gerlach, C. Holbrow, G. Huber, T. Kühl, D. Marx, K. Meier, P. Merz, W. Quint, F. Schmitt, M. Tomaselli, L. Völker, H. Winter, M. Würtz, K. Beckert, B. Franzke, F. Nolden, H. Reich, M. Steck, T. Winkler, Ground state hyperfine splitting of hydrogenlike $^{207}Pb^{81+}$ by laser excitation of a bunched ion beam in the GSI experimental storage ring. Phys. Rev. Lett. **81**, 4824 (1998)

193. W. Nörtershäuser, M. Lochmann, R. Jöhren, C. Geppert, Z. Andjelkovic, D. Anielski, B. Botermann, M. Bussmann, A. Dax, N. Frömmgen, M. Hammen, V. Hannen, T. Kühl, Y. A. Litvinov, J. Mader, T. Stöhlker, R. Thompson, C. Weinheimer, W. Wen, E. Will, D. Winters, R.M. Sánchez, Phys. Scr. 2013. 16th International Conference on the Physics of Highly Charged Ions (in print)
194. M.G.H. Gustavsson, A.-M. Mårtensson-Pendrill, Four decades of hyperfine anomalies. Adv. Quantum Chem. **30**(C), 343 (1998)
195. M.G.H. Gustavsson, A.-M. Mårtensson-Pendrill, Need for remeasurements of nuclear magnetic dipole moments. Phys. Rev. A: At. Mol. Opt. Phys. **58**, 3611 (1998)
196. V.M. Shabaev, A.N. Artemyev, V.A. Yerokhin, O.M. Zherebtsov, G. Soff, Towards a test of QED in investigations of the hyperfine splitting in heavy ions. Phys. Rev. Lett. **86**, 3959 (2001)
197. N.S. Oreshkina, D.A. Glazov, A. Volotka, V.M. Shabaev, I.I. Tupitsyn, Radiative and interelectronic-interaction corrections to the hyperfine splitting in highly charged B-like ions. Phys. Lett. A **372**(5), 675 (2008)
198. P. Beiersdorfer, T.W. Phillips, K.L. Wong, R.E. Marrs, D.A. Vogel, Measurement of level-specific dielectronic-recombination cross sections of heliumlike Fe XXV. Phys. Rev. A: At. Mol. Opt. Phys. **46**, 3812 (1992)
199. D.A. Knapp, R.E. Marrs, M.B. Schneider, M.H. Chen, M.A. Levine, P. Lee, Dielectronic recombination of heliumlike ions. Phys. Rev. A: At. Mol. Opt. Phys. **47**, 2039 (1993)
200. M.H. Chen, J.H. Scofield, Relativistic effects on angular distribution and polarization of dielectronic satellite lines of hydrogenlike ions. Phys. Rev. A: At. Mol. Opt. Phys. **52**, 2057 (1995)
201. M. Gail, N. Grün, W. Scheid, Angular distribution of radiation emitted after resonant transfer and excitation. J. Phys. B: At. Mol. Opt. Phys. **31**, 4645 (1998)
202. S. Zakowicz, Z. Harman, N. Grün, W. Scheid, Angular distribution of hypersatellite and satellite radiation emitted after resonant transfer and excitation into U^{91+} ions. Phys. Rev. A: At. Mol. Opt. Phys. **68**, 042711 (2003)
203. S. Zakowicz, W. Scheid, N. Grün, Dielectronic recombination into hydrogen-like heavy ions with emission of two photons. J. Phys. B: At. Mol. Opt. Phys. **37**, 131 (2004)
204. S. Fritzsche, N.M. Kabachnik, A. Surzhykov, Angular distribution of the dielectronic satellite lines from relativistic high-*Z* ions: Multipole-mixing effects. Phys. Rev. A: At. Mol. Opt. Phys. **78**, 032703 (2008)
205. S. Fritzsche, A. Surzhykov, Th Stöhlker, Dominance of the Breit interaction in the x-ray emission of highly charged ions following dielectronic recombination. Phys. Rev. Lett. **103**, 113001 (2009)
206. H.S.W. Massey, D.R. Bates, The properties of neutral and ionized atomic oxygen and their influence on the upper atmosphere. Rep. Progr. Phys. **9**, 62 (1942)
207. M.J. Seaton, P.J. Storey, *Di-electronic recombination* (North-Holland Publ. Co., Amsterdam, Netherlands, 1976)
208. D.A. Knapp, R.E. Marrs, M.A. Levine, C.L. Bennett, M.H. Chen, J.R. Henderson, M.B. Schneider, J.H. Scofield, Dielectronic recombination of heliumlike nickel. Phys. Rev. Lett. **62**, 2104 (1989)
209. T. Fuchs, C. Biedermann, R. Radtke, E. Behar, R. Doron, Channel-specific dielectronic recombination of highly charged krypton. Phys. Rev. A: At. Mol. Opt. Phys. **58**, 4518 (1998)
210. H. Watanabe, F.J. Currell, H. Kuramoto, Y.M. Li, S. Ohtani, B. O'Rourke, X.M. Tong, The measurement of the dielectronic recombination in He-like Fe ions. J. Phys. B: At. Mol. Opt. Phys. **34**, 5095 (2001)
211. H. Watanabe, H. Tobiyama, A.P. Kavanagh, Y.M. Li, N. Nakamura, H.A. Sakaue, F.J. Currell, S. Ohtani, Dielectronic recombination of He-like to C-like iodine ions. Phys. Rev. A: At. Mol. Opt. Phys. **75**, 012702 (2007)
212. B.E. O'Rourke, H. Kuramoto, Y.M. Li, S. Ohtani, X.M. Tong, H. Watanabe, F.J. Currell, Dielectronic recombination in He-like titanium ions. J. Phys. B: At. Mol. Opt. Phys. **37**, 2343 (2004)

213. A.J. Smith, P. Beiersdorfer, K. Widmann, M.H. Chen, J.H. Scofield, Measurement of resonant strengths for dielectronic recombination in heliumlike Ar^{16+}. Phys. Rev. A: At. Mol. Opt. Phys. **62**, 052717 (2000)
214. A.J. Smith, P. Beiersdorfer, V. Decaux, K. Widmann, K.J. Reed, M.H. Chen, Measurement of the contributions of high-n satellite lines to the $K\alpha$ lines of He-like Ar^{16+}. Phys. Rev. A: At. Mol. Opt. Phys. **54**, 462 (1996)
215. Y. Zou, J.R. Crespo, López-Urrutia, J. Ullrich, Observation of dielectronic recombination through two-electron-one-photon correlative stabilization in an electron-beam ion trap. Phys. Rev. A: At. Mol. Opt. Phys. **67**, 427031 (2003)
216. X. Zhang, J.R. Crespo, López-Urrutia, P. Guo, V. Mironov, X. Shi, A.J.G. Martinez, H. Tawara, J. Ullrich, Experimental study of the deep-lying dielectronic recombination resonances of He-like germanium ions. J. Phys. B: At. Mol. Opt. Phys. **37**, 2277 (2004)
217. Y. Hahn, Theory of dielectronic recombination. Adv. At. Mol. Opt. Phys. **21**(C), 123 (1985)
218. Y. Hahn, K.J. Lagattuta, Dielectronic recombination and related resonance processes. Phys. Rep. **166**, 195 (1988)
219. P. Zimmerer, N. Grün, W. Scheid, Auger rates for dielectronic recombination cross sections with highly charged relativistic heavy ions. Phys. Lett. Sect. A: Gen. At. Solid State Phys. **148**, 457 (1990)
220. P. Zimmerer, N. Grün, W. Scheid, Scaling of relativistic Auger rates with Z for ions with two electrons. J. Phys. B: At. Mol. Opt. Phys. **24**, 2633 (1991)
221. M. Zimmermann, N. Grün, W. Scheid, Photo recombination on highly charged few-electron uranium ions. J. Phys. B: At. Mol. Opt. Phys. **30**, 5259 (1997)
222. M.S. Pindzola, F.J. Robicheaux, N.R. Badnell, M.H. Chen, M. Zimmermann, Photorecombination of highly charged uranium ions. Phys. Rev. A: At. Mol. Opt. Phys. **52**, 420 (1995)
223. L.N. Labzowsky, A.V. Nefiodov, Radiative interference effects in the dielectronic-recombination process of an electron with hydrogenlike uranium. Phys. Rev. A: At. Mol. Opt. Phys. **49**, 236 (1994)
224. O.Y. Andreev, L.N. Labzowsky, G. Plunien, D.A. Solovyev, QED theory of the spectral line profile and its applications to atoms and ions. Phys. Rep. **455**, 135 (2008)
225. C. Beilmann, P.H. Mokler, S. Bernitt, C.H. Keitel, J. Ullrich, J.R. Crespo, López-Urrutia, Z. Harman, Prominent higher-order contributions to electronic recombination. Phys. Rev. Lett. **107**, 143201 (2011)
226. J.B. Mann, W.R. Johnson, Breit interaction in multielectron atoms. Phys. Rev. A: At. Mol. Opt. Phys. **4**, 41 (1971)
227. K.T. Cheng, M.H. Chen, J. Sapirstein, Quantum electrodynamic corrections in high-Z Li-like and Be-like ions. Phys. Rev. A: At. Mol. Opt. Phys. **62**, 054501 (2000)
228. H. Zhimin, X. Han, Y. Li, D. Kato, X. Tong, N. Nakamura, Experimental demonstration of the Breit interaction which dominates the angular distribution of x-ray emission in dielectronic recombination. Phys. Rev. Lett. **108**, 073002 (2012)
229. U. Fano, Effects of configuration interaction on intensities and phase shifts. Phys. Rev. **124**, 1866 (1961)
230. V.L. Jacobs, Theory of radiative corrections to Auger and fluorescence yields and dielectronic satellite line intensities. Phys. Rev. A: At. Mol. Opt. Phys. **31**, 383 (1985)
231. S.L. Haan, V.L. Jacobs, Projection-operator approach to the unified treatment of radiative and dielectronic recombination. Phys. Rev. A: At. Mol. Opt. Phys. **40**, 80 (1989)
232. S. Schippers, S. Kieslich, A. Müller, G. Gwinner, M. Schnell, A. Wolf, A. Covington, M.E. Bannister, L.-B. Zhao, Interference effects in the photorecombination of argonlike Sc^{3+} ions: Storage-ring experiment and theory. Phys. Rev A: At. Mol. Opt. Phys. **65**, 042723 (2002)
233. V.V. Karasiov, L.N. Labzowsky, A.V. Nefiodov, V.M. Shabaev, Overlapping resonances in the process of recombination of an electron with hydrogenlike uranium. Phys. Lett. Sect. A: Gen. At. Solid State Phys. **161**, 453 (1992)
234. A.V. Nefiodov, V.V. Karasiev, V.A. Yerokhin, Interference effects in the recombination process of hydrogenlike lead. Phys. Rev. A: At. Mol. Opt. Phys. **50**, 4975 (1994)

235. D.A. Knapp, P. Beiersdorfer, M.H. Chen, J.H. Scofield, D. Schneider, Observation of interference between dielectronic recombination and radiative recombination in highly charged uranium ions. Phys. Rev. Lett. **74**, 54 (1995)
236. N. Nakamura, A.P. Kavanagh, H. Watanabe, H.A. Sakaue, Y. Li, D. Kato, F.J. Currell, X.-M. Tong, T. Watanabe, S. Ohtani, Asymmetric profiles observed in the recombination of Be^{79+}: A benchmark for relativistic theories involving interference. Phys. Rev. A: At. Mol. Opt. Phys. **80**, 014503 (2009)
237. A. J. González Martínez, J.R. Crespo López-Urrutia, J. Braun, G. Brenner, H. Bruhns, A. Lapierre, V. Mironov, R. Soria Orts, H. Tawara, M. Trinczek, J. Ullrich, A.N. Artemyev, Z. Harman, U.D. Jentschura, C.H. Keitel, J.H. Scofield, I.I. Tupitsyn, Benchmarking high-field few-electron correlation and QED contributions in Hg^{75+} to Hg^{78+} ions. I. Experiment. Phys. Rev. A: At. Mol. Opt. Phys. **73**, 052710 (2006)
238. M.F. Gu, T. Holczer, E. Behar, S.M. Kahn, Inner-shell absorption lines of Fe VI–Fe XVI: A many-body perturbation theory approach. Astrophys. J. **641**, 1227 (2006)
239. S.W. Epp, J.R. Crespo, López-Urrutia, M. C. Simon, T. Baumann, G. Brenner, R. Ginzel, N. Guerassimova, V. Mäckel, P.H. Mokler, B.L. Schmitt, H. Tawara, J. Ullrich, X-ray laser spectroscopy of highly charged ions at FLASH. J. Phys. B: At. Mol. Opt. Phys. **43**, 194008 (2010)
240. D.L. Matthews, P.L. Hagelstein, M.D. Rosen, M.J. Eckart, N.M. Ceglio, A.U. Hazi, H. Medecki, B.J. MacGowan, J.E. Trebes, B.L. Whitten, E.M. Campbell, C.W. Hatcher, A.M. Hawryluk, R.L. Kauffman, L.D. Pleasance, G. Rambach, J.H. Scofield, G. Stone, T.A. Weaver, Demonstration of a soft x-ray amplifier. Phys. Rev. Lett. **54**, 110 (1985)
241. M.D. Rosen, P.L. Hagelstein, D.L. Matthews, E.M. Campbell, A.U. Hazi, B.L. Whitten, B. MacGowan, R.E. Turner, R.W. Lee, G. Charatis, Gar. E. Busch, C. L. Shepard, P. D. Rockett, Exploding-foil technique for achieving a soft x-ray laser. Phys. Rev. Lett. **54**, 106 (1985)
242. J.J. Rocca, V. Shlyaptsev, F.G. Tomasel, O.D. Cortzar, D. Hartshorn, J.L.A. Chilla, Demonstration of a discharge pumped table-top soft-x-ray laser. Phys. Rev. Lett. **73**, 2192 (1994)
243. J. Andruszkow, B. Aune, V. Ayvazyan, N. Baboi, R. Bakker, V. Balakin, D. Barni, A. Bazhan, M. Bernard, A. Bosotti, J.C. Bourdon, W. Brefeld, R. Brinkmann, S. Buhler, J.-P. Carneiro, M. Castellano, P. Castro, L. Catani, S. Chel, Y. Cho, S. Choroba, E.R. Colby, W. Decking, P. Den Hartog, M. Desmons, M. Dohlus, D. Edwards, H.T. Edwards, B. Faatz, J. Feldhaus, M. Ferrario, M.J. Fitch, K. Flöttmann, M. Fouaidy, A. Gamp, T. Garvey, C. Gerth, M. Geitz, E. Gluskin, V. Gretchko, U. Hahn, W.H. Hartung, D. Hubert, M. Hüning, R. Ischebek, M. Jablonka, J.M. Joly, M. Juillard, T. Junquera, P. Jurkiewicz, A. Kabel, J. Kahl, H. Kaiser, T. Kamps, V.V. Katelev, J.L. Kirchgessner, M. Körfer, L. Kravchuk, G. Kreps, J. Krzywinski, T. Lokajczyk, R. Lange, B. Leblond, M. Leenen, J. Lesrel, M. Liepe, A. Liero, T. Limberg, R. Lorenz, L.H. Hua, L.F. Hai, C. Magne, M. Maslov, G. Materlik, A. Matheisen, J. Menzel, P. Michelato, W.-D. Möller, A. Mosnier, U.-C. Müller, O. Napoly, A. Novokhatski, M. Omeich, H.S. Padamsee, C. Pagani, F. Peters, B. Petersen, P. Pierini, J. Pflüger, P. Piot, B. Phung, Ngoc, L. Plucinski, D. Proch, K. Rehlich, S. Reiche, D. Reschke, I. Reyzl, J. Rosenzweig, J. Rossbach, S. Roth, E. L. Saldin, W. Sandner, Z. Sanok, H. Schlarb, G. Schmidt, P. Schmüser, J. R. Schneider, E. A. Schneidmiller, H.-J. Schreiber, S. Schreiber, P. Schütt, J. Sekutowicz, L. Serafini, D. Sertore, S. Setzer, S. Simrock, B. Sonntag, B. Sparr, F. Stephan, V.A. Sytchev, S. Tazzari, F. Tazzioli, M. Tigner, M. Timm, M. Tonutti, E. Trakhtenberg, R. Treusch, D. Trines, V. Verzilov, T. Vielitz, V. Vogel, G.V. Walter, R. Wanzenberg, T. Weiland, H. Weise, J. Weisend, M. Wendt, M. Werner, M.M. White, I. Will, S. Wolff, M.V. Yurkov, K. Zapfe, P. Zhogolev, F. Zhou, First observation of self-amplified spontaneous emission in a free-electron laser at 109 nm wavelength. Phys. Rev. Lett. **85**, 3825 (2000)
244. C. Bostedt, H.N. Chapman, J.T. Costello, J.R. Crespo, López-Urrutia, S. Düsterer, S.W. Epp, J. Feldhaus, A. Föhlisch, M. Meyer, T. Möller, R. Moshammer, M. Richter, K. Sokolowski-Tinten, A. Sorokin, K. Tiedtke, J. Ullrich, W. Wurth, Experiments at FLASH. Nucl. Instrum. Methods Phys. Res. Sect. A **601**, 108 (2009)

245. H.-C. Wille, H. Franz, R. Röhlsberger, W. Caliebe, F.-U. Dill, Nuclear resonant scattering at PETRA III : Brillant opportunities for nano− and extreme condition science. J. Phys: Conf. Ser. **217**, 012008 (2009)
246. U.I. Safronova, A.S. Safronova, W.R. Johnson, Relativistic many-body calculations of dielectronic satellite spectra created by autoionizing $1s2l2l'$ states in Li-like ions. J. Phys. B: At. Mol. Opt. Phys. **43**(14), 144001 (2010)
247. A.S. Shlyaptseva, R.C. Mancini, P. Neill, P. Beiersdorfer, J.R. Crespo, López-Urrutia, K. Widmann, Polarization-dependent spectra of x-ray dielectronic satellite lines of Be-like Fe. Phys. Rev. A: At. Mol. Opt. Phys. **57**, 888 (1998)
248. T.V. Back, H.S. Margolis, P.K. Oxley, J.D. Silver, E.G. Myers, Laser spectroscopy of the $1s^2 2s2p\,^3P_2$–$^3P_1$ transition in beryllium-like argon using the Oxford EBIT. Hyperfine Interact. **114**, 203 (1998)
249. D. Schneider, D.A. Church, G. Weinberg, J. Steiger, B. Beck, J. McDonald, E. Magee, D. Knapp, Confinement in a cryogenic penning trap of highest charge state ions from EBIT. Rev. Sci. Instrum. **65**, 3472 (1994)
250. V. Mäckel, R. Klawitter, G. Brenner, J.R. Crespo, López-Urrutia, J. Ullrich, Laser spectroscopy on forbidden transitions in trapped highly charged Ar^{13+} ions. Phys. Rev. Lett. **107**, 143002 (2011)
251. K. Schnorr, V. Mäckel, N.S. Oreshkina, S. Augustin, F. Brunner, Z. Harman, C.H. Keitel, J. Ullrich, J.R. Crespo López-Urrutia, Coronium in the laboratory: measuring the Fe XIV green coronal line by laser spectroscopy. Astrophys. J. **776**(2), 121 (2013)
252. C.A. Young, The Sun and the phenomena of its atmosphere (C.C. Chatfield & Co., New Haven, Connecticut, 1872)
253. W. Grotrian, Zur Frage der Deutung der Linien im Spektrum der Sonnenkorona. Naturwissenschaften **27**(13), 214 (1939)
254. B. Edlén, Die Deutung der Emissionslinien im Spektrum der Sonnenkorona. Mit 6 Abbildungen. Zeitschrift für Astrophysik **22**, 30 (1943)
255. S.A. Diddams, Th Udem, J.C. Bergquist, E.A. Curtis, R.E. Drullinger, L. Hollberg, W.M. Itano, W.D. Lee, C.W. Oates, K.R. Vogel, D.J. Wineland, An optical clock based on a single trapped $^{199}Hg^+$ ion. Science **293**, 825 (2001)
256. K.T. Cheng, M.H. Chen, W.R. Johnson, J. Sapirstein, High-precision relativistic atomic structure calculations and the EBIT: Tests of quantum electrodynamics in highly charged ions. Can. J. Phys. **86**, 33 (2008)
257. T. Rosenband, P.O. Schmidt, D.B. Hume, W.M. Itano, T.M. Fortier, J.E. Stalnaker, K. Kim, S.A. Diddams, J.C.J. Koelemeij, J.C. Bergquist, D.J. Wineland, Observation of the $^1S_0$–$^3P_0$ clock transition in Al^+. Phys. Rev. Lett. **98**, 220801 (2007)
258. C.W. Chou, D.B. Hume, J.C.J. Koelemeij, D.J. Wineland, T. Rosenband, Frequency comparison of two high-accuracy Al^+ optical clocks. Phys. Rev. Lett. **104**, 070802 (2010)
259. C.J. Campbell, A.G. Radnaev, A. Kuzmich, V.A. Dzuba, V.V. Flambaum, A. Derevianko, Single-ion nuclear clock for metrology at the 19th decimal place. Phys. Rev. Lett. **108**, 120802 (2012)
260. K. Hosaka, S.A. Webster, A. Stannard, B.R. Walton, H.S. Margolis, P. Gill, Frequency measurement of the $^2S_{1/2}$–$^2F_{7/2}$ electric octupole transition in a single $^{171}Yb^+$ ion. Phys. Rev. A: At. Mol. Opt. Phys. **79**, 033403 (2009)
261. A.L. Wolf, S.A. Van Den Berg, W. Ubachs, K.S.E. Eikema, Direct frequency comb spectroscopy of trapped ions. Phys. Rev. Lett. **102**, 223901 (2009)
262. D.Z. Kandula, C. Gohle, T.J. Pinkert, W. Ubachs, K.S.E. Eikema, Extreme ultraviolet frequency comb metrology. Phys. Rev. Lett. **105**, 063001 (2010)
263. A. Cingaz, D.C. Yost, T.K. Allison, A. Ruehl, M.E. Fermann, I. Hartl, J. Ye, Direct frequency comb spectroscopy in the extreme ultraviolet. Nature **482**, 68 (2012)
264. J.B. Wübbena, S. Amairi, O. Mandel, P.O. Schmidt, Sympathetic cooling of mixed-species two-ion crystals for precision spectroscopy. Phys. Rev. A: At. Mol. Opt. Phys. **85**, 043412 (2012)

265. V.V. Flambaum, J.C. Berengut, Space-time variation of coupling constants and fundamental masses. Int. J. Modern Phys. A **24**, 3342 (2009)
266. J.C. Berengut, V.A. Dzuba, V.V. Flambaum, Enhanced laboratory sensitivity to variation of the fine-structure constant using highly charged ions. Phys. Rev. Lett. **105**, 120801 (2010)
267. S. Schiller, Hydrogenlike highly charged ions for tests of the time independence of fundamental constants. Phys. Rev. Lett. **98**, 180801 (2007)
268. J.C. Berengut, V.A. Dzuba, V.V. Flambaum, A. Ong, Electron-hole transitions in multiply charged ions for precision laser spectroscopy and searching an α: for variations in α. Phys. Rev. Lett. **106**, 210802 (2011)
269. J.C. Berengut, V.A. Dzuba, V.V. Flambaum, A. Ong, Optical transitions in highly charged californium ions with high sensitivity to variation of the fine-structure constant. Phys. Rev. Lett. **109**, 070802 (2012)
270. J.C. Berengut, V.A. Dzuba, V.V. Flambaum, A. Ong, Highly charged ions with E1, M1, and E2 transitions within laser range. Phys. Rev. A: At. Mol. Opt. Phys. **86**, 022517 (2012)
271. V.A. Dzuba, A. Derevianko, V.V. Flambaum, Ion clock and search for the variation of the fine-structure constant using optical transitions in Nd^{13+} and Sm^{15+}. Phys. Rev. A: At. Mol. Opt. Phys. **86**, 054502 (2012)
272. V.A. Dzuba, A. Derevianko, V.V. Flambaum, High-precision atomic clocks with highly charged ions: Nuclear-spin-zero f^{12}-shell ions. Phys. Rev. A: At. Mol. Opt. Phys. **86**, 054501 (2012)
273. A. Derevianko, V.A. Dzuba, V.V. Flambaum, Highly charged ions as a basis of optical atomic clockwork of exceptional accuracy. Phys. Rev. Lett. **109**, 180801 (2012)
274. L. Gruber, J.P. Holder, J. Steiger, B.R. Beck, H.E. DeWitt, J. Glassman, J.W. McDonald, D.A. Church, D. Schneider, Evidence for highly charged ion coulomb crystallization in multicomponent strongly coupled plasmas. Phys. Rev. Lett. **86**, 636 (2001)
275. M. Schwarz, O.O. Versolato, A. Windberger, F.R. Brunner, T. Ballance, S.N. Eberle, J. Ullrich, P.O. Schmidt, A.K. Hansen, A.D. Gingell, M. Drewsen, J.R. Crespo, López-Urrutia. Cryogenic linear Paul trap for cold highly charged ion experiments. Rev. Sci. Instrum. **83**, 083115 (2012)
276. O. O. Versolato, M. Schwarz, A.K. Hansen, A,D. Gingell, A. Windberger, L. Klosowski, J. Ullrich, F. Jensen, J.R. Crespo, M. López-Urrutia Drewsen, Decay rate measurement of the first vibrationally excited state of MgH^+ in a cryogenic Paul trap. Phys. Rev. Lett. **111**(5), 053002 (2013)
277. O.O. Versolato, M. Schwarz, A. Windberger, J. Ullrich, P.O. Schmidt, M. Drewsen, J.R. Crespo, López-Urrutia, Cold highly charged ions in a cryogenic paul trap. Hyperfine Interact. **214**, 189 (2013)
278. P.O. Schmidt, T. Rosenband, C. Langer, W.M. Itano, J.C. Bergquist, D.J. Wineland, Physics: Spectroscopy using quantum logic. Science **309**(5735), 749 (2005)
279. D.B. Hume, C.W. Chou, D.R. Leibrandt, M.J. Thorpe, D.J. Wineland, T. Rosenband, Trapped-ion state detection through coherent motion. Phys. Rev. Lett. **107**, 243902 (2011)
280. D.J. Wineland, D. Leibfried, Quantum information processing and metrology with trapped ions. Laser Phys. Lett. **8**, 175 (2011)
281. B.W. Adams, C. Buth, S.M. Cavaletto, J. Evers, Z. Harman, C.H. Keitel, A. Pálffy, A. Picón, R. Röhlsberger, Y. Rostovtsev, K. Tamasaku, X-ray quantum optics. J. Modern Opt. **60**, 2–21 (2013)
282. C.R. Clark, J.E. Goeders, Y.K. Dodia, C.R. Viteri, K.R. Brown, Detection of single-ion spectra by Coulomb-crystal heating. Phys. Rev. A: At. Mol. Opt. Phys. **81**, 043428 (2010)
283. A. Pálffy, Nuclear effects in atomic transitions. Contemp. Phys. **51**, 471 (2010)
284. J.N. Tan, S.M. Brewer, N.D. Guise, Experimental efforts at NIST towards one-electron ions in circular Rydberg states. Phys. Scr. T **144**, 014009 (2011)